

Energetics of charged metal clusters containing vacancies

Valentin V. Pogosov* and Vitalii I. Reva
*Zaporozh'ye National Technical University,
69063 Zaporozh'ye, Zhukovsky Str. 64, Ukraine
vpogosov@zntu.edu.ua*

(Dated: September 22, 2018)

We study theoretically large metal clusters containing vacancies. We propose an approach, which combines the Kohn-Sham results for monovacancy in a bulk of metal and analytical expansions in small parameters c_v (relative concentration of vacancies) and $R_{N,v}^{-1}$, $R_{N,v}$ being cluster radius. We obtain expressions of the ionization potential and electron affinity in the form of corrections to electron work function, which require only the characteristics of 3D defect-free metal.

The Kohn-Sham method is used to calculate the electron profiles, ionization potential, electron affinity, electrical capacitance; dissociation, cohesion and monovacancy-formation energies of the small perfect clusters Na_N , Mg_N , Al_N ($N \leq 270$) and the clusters containing a monovacancy ($N \geq 12$) in the stabilized-jellium model. The quantum-sized dependences for monovacancy-formation energies are calculated for the Schottky scenario and the “bubble blowing” scenario, and their asymptotic behavior is also determined. It is shown that the asymptotical behaviors of size dependences for these two mechanisms differ from each other and weakly depend on the number of atoms in the cluster. The contribution of monovacancy to energetics of charged clusters, the size dependences of their characteristics and asymptotics is discussed. It is shown that difference between the characteristics for the neutral and charged cluster is entirely determined by size dependences of ionization potential and electron affinity. Obtained analytical dependences may be useful for the analysis of the results of photoionization experiments and for the estimation of the size dependences of the vacancy concentration including the vicinity of the melting point.

PACS numbers: 73.61.At, 36.40.Vz, 68.55.Ln, 68.65.Cd, 71.15.Mb, 73.30.+y, 32.10.Hq

I. INTRODUCTION

Frenkel theory of melting assumes an abrupt increase of the vacancies concentration at the triple point, as well as the decrease in monovacancy-formation energies with increasing their concentration [1–3]. The equilibrium vacancy concentration is estimated from thermodynamic considerations based on the monovacancy-formation energy, the magnitude of which, in turn, can be extracted from positron annihilation spectroscopy [4]. At the melting point, the relative concentration of vacancies in metals is a fraction of a percent. Despite such small concentrations, vacancies significantly influence properties of solids. In the case of radiation damage in 3D metals or metal islands, the vacancy concentration can be even tens of percent.

Small metal nanoclusters at low temperatures can be in superconducting state, which results in a strong modification of the energy spectrum. It is known that superconducting correlations depend crucially on the density of states near the Fermi energy. Certain shapes of nanoclusters support highly enhanced density of states near electronic shell closings, see, e.g., recent works [5, 6]. For ideal nanoclusters, the highest energy occupied electronic levels become strongly degenerate at spherical shell closings (“magic” numbers). The presence of vacancies, as shown below, will lead to a change in the magic numbers

of atoms and might result in smearing of the effect of shell structure on superconducting correlations including gap in excitation spectrum.

Initially, in the experiments it was established that the temperature melting of clusters on a substrate and free clusters decreases with a decrease in their size [7, 8]. Interpretations of this mesoscopic phenomena were developed in a number of papers [9–15]. A popular point of view is based on thermodynamical considerations: near the temperature melting – the smaller cluster size, the lower a monovacancy-formation energy while the vacancy concentration is not size- dependent [9, 11].

Modern mass spectroscopic and calorimetric methods, allowing to study in detail the process of premelting and postmelting in metal clusters consisting of a countable number of atoms [16–19], have shown that the melting temperature is characterized by an oscillatory size dependence, and also has dimensional anomalies (for example, for Al), poorly described by simple models [16, 18]. Also, in the melting process the diffusion of surface vacancies into bulk is more favorable for clusters with unfilled electronic shells than for clusters with the magic number of atoms [17]. These facts stimulate growing interest in the description of phase transition from the solid to the liquid state, as the configuration excitation of voids-vacancies in the clusters. For example, the question about the size of the monovacancy-formation energies, the vacancy concentration and a relation to the melting process remains open.

For the first time, mass-spectrometric measurements of dissociation energy cluster ions Na_N^+ were reported in

*Corresponding author: vpogosov@zntu.edu.ua

[20], and for Al_N^+ in [21]. Traditionally, according to such data, and also based on the measured ionization potentials, the cohesion energy of neutral clusters is calculated.

Recently, the ionization potential of Al_{32-95} clusters and its temperature dependence in the range 65 – 230 K were measured in [22]. With increasing temperature, a decrease of the ionization potential is not significant (~ 10 meV). The melting point of such clusters is in the range 600 – 700 K [16, 18].

The energy characteristics of solid clusters have been intensively studied within different models and approaches, including triaxially deformed ordinary jellium and *ab initio* simulations (see [23–29] and references therein). We use model of spherical stabilized jellium [30] that does not contain adjustable parameters. It is also convenient and transparent for the analysis of the role played by vacancies in cluster melting or other excitation processes.

However, with the exception of the works [31, 32], self-consistent calculations for monovacancy-formation energy in clusters and the impact on it of electronic spectrum quantization has not yet been addressed. Therefore, one of the actual problems that can be formulated in connection with melting of small-sized aggregates, is the study of the size of its electron affinity and ionization potential in the case of clusters contained vacancies. In our model, the monovacancy is represented in the form of spherical void of atomic size in a homogeneous positively charged background due to the ions [31, 33].

An electron binding energy for small perfect clusters may be calculated numerically only. In the opposite case of large clusters the binding energy is close to the binding energy for the 3D metal with the first size correction due to surface curvature. In [25, 34, 35] an exhaustive survey of the semiclassical description of IP and EA in the form of the first dimensional correction to the work function is given. In our work the second size corrections are also taken into account and the developed procedure is suitable for calculations of the ionization potential and electron affinity of metal clusters containing point defects and impurities. As an example, vacancies are considered. This approach can be easily adapted for calculation of the positron attachment energy for such clusters.

We propose a method, which combines several approaches. The first one is based on a density-functional solution in the stabilized jellium model for metal monovacancy in the bulk ignoring an external surface. This problem was addressed by us earlier. We found a shift in the energy of the ground state of the electrons [36] and positrons [37] due to the presence of a “subsystem” of vacancies in 3D metal.

In the first approximation it is assumed that vacancies are noninteracting because of their small concentration. However, there are experiments showing that in some metallic systems the partial ordering of vacancies is observed [38], i.e. the energy of vacancies formation has to be concentration dependent.

The second one uses a solution for a defect-free metal

in presence of an external flat surface, but with lower atomic density. The lower density of the atoms is due to the existence of superlattice of vacancies of relative concentration c_v in the defected metal. Using c_v as a small parameter, all metal characteristics are evaluated as series expansions. In these expansions the zero-order terms are the characteristics of defect-free metal, and the first-order terms are expressed through them. This approach allows to obtain the vacancy dependence of electron work function for 3D metal. These results are then used to evaluate an asymptotic size dependence of the ionization potential of a spherical metal cluster and the electron affinity.

The consistent procedure for the calculation of a size dependence of ionization potential and electron affinity of a large spherical metal cluster containing vacancies is presented. In the framework of effective medium approach, the perturbation theory over the small parameters c_v , $R_v/R_{N,v}$ and L_v/R_v is proposed for the ionization potential and electron affinity (R_v is the average distance between vacancies and L_v is the electron-vacancy scattering length).

For small clusters Rb, K, Na, Li, Mg and Al containing monovacancy we performed the Kohn-Sham calculations of the electron and effective potential profiles; the ionization potential and an electron affinity; the dissociation, the cohesion, the vacancy formation energies. For demonstration and analysis of results, we limited ourselves to metals Na, Mg and Al.

The size dependences for monovacancy-formation energies are calculated for the Schottky scenario and the “bubble blowing” scenario, and their asymptotic behavior is also determined. It is shown that the asymptotical behaviors of size dependences for these two mechanisms differ from each other and weakly depend on the number of atoms in the cluster. The contribution of monovacancy to energetics of charged clusters, the size dependences of their characteristics and asymptotics is discussed. It is shown that difference between the characteristics for the neutral and charged cluster is entirely determined by size dependences of ionization potential and electron affinity.

II. IONIZATION POTENTIAL AND ELECTRON AFFINITY

A. General relation

By definition, the ionization potential and the electron affinity of a metal cluster with the N atoms and radius

$$R_N = N^{1/3}r_0, \quad (1)$$

where r_0 is the radius of Wigner-Seitz cell per unit atom, have the form

$$\begin{aligned} \text{IP}_N &= E_N^+(R_N) - E_N(R_N), \\ \text{EA}_N &= E_N(R_N) - E_N^-(R_N), \end{aligned} \quad (2)$$

where $E_N^+ \equiv E_N^{N_e-1}$, $E_N^- \equiv E_N^{N_e+1}$ and E_N are total energies of charged and neutral spheres; $N_e = ZN$ is the total number of electrons in a neutral cluster, Z is a valency of metal.

The basis of the semiclassical approximation is the expansion of the electron chemical potential μ of valence electrons and the surface energy per unit area σ of the neutral cluster in powers of the inverse radius R_N^{-1} (liquid drop model) [39, 40]:

$$\begin{aligned}\mu(R_N) &= \mu_0 + \frac{\mu_1}{R_N} + \frac{\mu_2}{R_N^2} + O(R_N^{-3}), \\ \sigma(R_N) &= \sigma_0 + \frac{\sigma_1}{R_N} + \frac{\sigma_2}{R_N^2} + O(R_N^{-3}),\end{aligned}\quad (3)$$

where μ_0 and σ_0 correspond to flat surface ($R_N \rightarrow \infty$).

From the condition of mechanical equilibrium of the cluster, the sum rules were obtained in Refs. [41–44]. In particular

$$\begin{aligned}\mu_1 &= \frac{2\sigma_0}{\bar{n}}, \\ \mu_2 &= \mu_1 \left(\delta_1 - \frac{\sigma_0}{B_0} \right),\end{aligned}\quad (4)$$

where $\delta_1 = \sigma_1/\sigma_0$. Next, it is convenient to use the values $\tilde{\mu}_1 \equiv \mu_1/r_0$, $\tilde{\mu}_2 \equiv \mu_2/r_0^2$ having a dimension of energy.

Consider a metallic cluster consisting of N atoms and containing N_v vacancies. Then radius of the cluster is

$$R_{N,v} = R_N (1 + c_v)^{1/3}, \quad c_v = N_v/N. \quad (5)$$

Clusters of atoms have a structural periodicity, which is not translational, but rather has a property of “spherical periodicity” [45]. This periodicity is due to spherical layers of atoms (atomic shells or coordination spheres). By this principle, one can also consider the vacancy “subsystem” in a cluster with distribution over spherical layers. We divide conditionally the cluster into N_v Wigner-Seitz supercells of radius

$$R_v = \left(\frac{3}{4\pi n_a c_v} \right)^{1/3} \gg r_0 = \left(\frac{3}{4\pi n_a} \right)^{1/3}, \quad (6)$$

where n_a is the concentration of atoms. Respectively the supercellular “muffin-tin” potential is replaced by a spherical symmetric one.

For a large cluster with dilute subsystem of vacancies, we will use the expressions

$$\begin{aligned}\text{IP}_{N,v} &= W_{\text{eff},v} - \frac{\mu_1}{R_{N,v}} - \frac{\mu_2}{R_{N,v}^2} + \frac{e^2}{2C_{N,v}}, \\ \text{EA}_{N,v} &= W_{\text{eff},v} - \frac{\mu_1}{R_{N,v}} - \frac{\mu_2}{R_{N,v}^2} - \frac{e^2}{2C_{N,v}},\end{aligned}\quad (7)$$

where $W_{\text{eff},v}$ is the effective electron work function of 3D metal containing vacancies, $-e$ is the electron charge. The last term (7) is the charging energy of metallic sphere with electric capacitance

$$C_{N,v} = R_{N,v}. \quad (8)$$

The analysis of experimental data for small metallic clusters is usually carried out according to the formulae

$$\begin{aligned}\text{IP}_N &= W_0 + \frac{\alpha e^2}{N^{1/3}}, \quad \alpha = \frac{1}{2r_0} - \frac{\tilde{\mu}_1}{e^2}, \\ \text{EA}_N &= W_0 - \frac{\beta e^2}{N^{1/3}}, \quad \beta = \frac{1}{2r_0} + \frac{\tilde{\mu}_1}{e^2},\end{aligned}\quad (9)$$

which will be used by us as reference expressions.

B. Volume term for vacancy shift of the grand energy of electrons

The translational symmetry of the lattice of a solid is at the basis of calculation of the electron work functions. Therefore, to take into account the contribution of vacancies to work function, we have to assume their periodic location in the form of a “superlattice” in a metal. In this case the vacancy shift of the bottom of the electron conductivity band can be introduced.

The problem of description of our system within simple models is that the bulk of the metal is not homogeneous due to vacancies, so the density functional method in the jellium model must be solved as a three-dimensional problem. Within the one-dimensional problem, it is impossible to describe a set of spherically symmetric vacancies and a planar external metal surface.

The wave function of the ground state of the electron is determined by the Schrödinger equation

$$-\frac{\hbar^2}{2m} \nabla^2 \Psi(\mathbf{r}) + \left[v_{\text{eff}}(r) + \sum_{i=1}^{N_v} \delta v_{\text{eff},v}(\mathbf{r} - \mathbf{R}_i) \right] \Psi(\mathbf{r}) = \varepsilon_b \Psi(\mathbf{r}), \quad (10)$$

in which the vacancies are centered at the points \mathbf{R}_i ($R_i < R_{N,v}$). One-electron effective potentials are represented in such manner that the spherically symmetric potential $v_{\text{eff}}(r)$ forms the bottom of the conduction band and the surface barrier, and $\delta v_{\text{eff},v}(\mathbf{r} - \mathbf{R}_i)$ forms the i th vacancy (Fig. 1). In (10) the energy ε_b is a shift in the bottom of the conduction band due to the presence of vacancies.

Suppose that in 3D metal the potential field of the supercell has translational periodicity. Then the electron wave function of the ground state can be written in the form,

$$\Psi(\mathbf{r}) = \psi(\mathbf{r})u(\mathbf{r}), \quad (11)$$

where the function $\psi(\mathbf{r})$ (for 3D metal it is $e^{i\mathbf{k}\mathbf{r}}$) is modulated on the vacancy scale by the function $u(\mathbf{r})$. The function $u(\mathbf{r})$ is the superposition of the usual Wigner-Seitz solutions $u_{\text{WS}}(|\mathbf{r} - \mathbf{R}_i|)$ inside cells, centered at \mathbf{R}_i .

Next, ε_b can be represented as the sum

$$\varepsilon_b = \varepsilon^{(0)} + \varepsilon^{(1)}, \quad (12)$$

$$\varepsilon^{(0)} = T_0 + \langle \delta v_{\text{eff},v} \rangle_{R_v}, \quad (13)$$

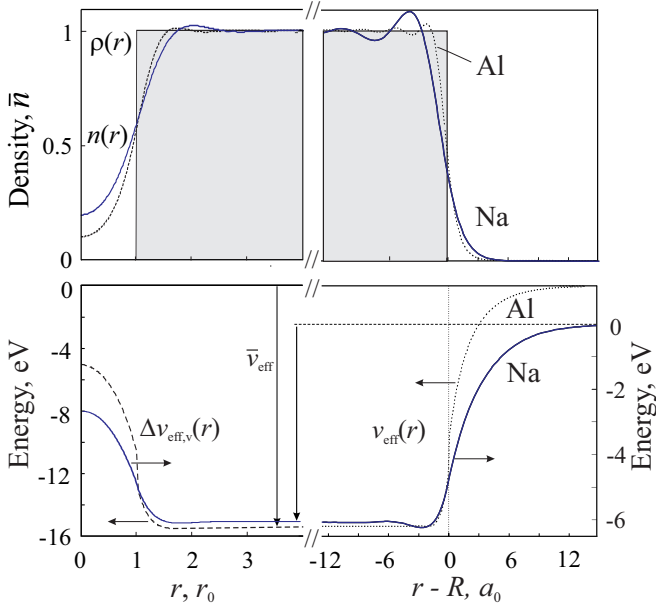


Figure 1: The calculated in [36] electron and effective potential profiles both near monovacancy in the bulk and planar surface ($R \rightarrow \infty$) for Na (blue solid line) and Al (black dashed line).

where T_0 is the cellular energy eigenvalue; $\langle \delta v_{\text{eff},v} \rangle_{R_v}$ is averaged over the volume of the supercell the contribution of potential energy from the electron-vacancy potential $\delta v_{\text{eff},v}(r) = v_{\text{eff},v}(r) - \bar{v}_{\text{eff}}$, where \bar{v}_{eff} is the position of the bottom of the conduction band in absence of vacancies (Fig. 1).

The value T_0 is determined from equation for supercell

$$\left[-\frac{\hbar^2}{2m} \nabla^2 + \delta v_{\text{eff},v}(r) - T_0 \right] u_{\text{WS}}(r) = 0 \quad (14)$$

with the boundary conditions

$$\nabla u_{\text{WS}}(r)|_{r=R_v} = 0, \quad u_{\text{WS}}(r)|_{r=L_v} = 0, \quad (15)$$

where L_v is the scattering length of electron on the vacancy (Table I). For an electron, the vacancy represents a potential hillock, therefore $L_v > 0$.

Table I. The results of the Kohn-Sham calculation of L_v for the electron scattering on monovacancy [36, 46].

Metal	Cs	Rb	K	Na	Li	Cu	Mg	Zn	Al	Pb
Z	1	1	1	1	1	2	2	3	3	4
r_s, a_0	5.63	5.2	4.86	3.99	3.28	2.11	2.65	2.31	2.07	2.30
L_v, a_0	4.85	2.38	2.26	1.85	1.52	1.56	2.02	2.10	1.93	2.47

Substitution of the expression for the electron wave function

$$u_{\text{WS}}(r) = \frac{A}{\sqrt{4\pi}} \frac{\sin[q_0(r - L_v)]}{q_0 r} \quad (16)$$

in the second boundary condition gives the equation

$$\tan[q_0(R_v - L_v)] - q_0 R_v = 0, \quad (17)$$

from which we obtain

$$T_0 = \frac{\hbar^2 q_0^2}{2m}. \quad (18)$$

This approach was first used in [47].

The interaction of an electron with vacancies can also be described using the Fermi optical approximation

$$T_0 = \frac{3\hbar^2 L_v}{2m r_0^3} c_v. \quad (19)$$

Here it should be noted that the smaller c_v the better agreement between results of calculations using (16) (18) and (19). Solving Eqs. (17) and (19), for example, for Al with $c_v = 0.01$ leads to the values $T_0 = 0.0388$ eV and 0.0296 eV, respectively, which evidences that an accuracy of the optical approximation is lower.

The value of T_0 is determined by the s -phase of scattering ($\rightarrow -L_v k$ as $k \rightarrow 0$) for $k = q_0$ and can be tested by the value of residual resistivity of vacancies. All phases of electron scattering for a monovacancy give contributions to the resistivity, but the main contribution is produced by the s -phase of scattering for $k = k_F$ (see Table 1 in [36]). The residual resistivity of vacancies estimated in [36] turned out to be 2-3 times lower than the experimental values.

The value $\langle \delta v_{\text{eff},v} \rangle_{R_v}$ in (13) is determined in the mean-field approximation by the expression

$$\langle \delta v_{\text{eff},v} \rangle_{R_v} = \frac{3c_v}{4\pi r_0^3} \int_0^{R_v} dr 4\pi r^2 \delta v_{\text{eff},v}(r), \quad (20)$$

in which it is convenient to substitute $R_v = r_0 c_v^{-1/3}$.

Using the numerical solution of the problem of electron scattering on the vacancy potential [36] we get

$$\varepsilon^{(0)} = A_1 c_v + O(c_v^2), \quad (21)$$

where $A_1 = 4.10$ eV and 13.3 eV for Na and Al, respectively.

We substitute (11) and (14) into the equation (10), which after simple transformations can be rewritten in the form

$$\left[-\frac{\hbar^2}{2m} \nabla^2 - \frac{\hbar^2}{m} \sum_{i=1}^{N_v} \frac{\nabla u_{\text{WS}}(\varrho)}{u_{\text{WS}}(\varrho)} \nabla + v_{\text{eff}}(r) - \varepsilon^{(1)} \right] \psi(\mathbf{r}) = 0, \quad (22)$$

where $\varrho \equiv |\mathbf{r} - \mathbf{R}_i|$.

The Eq. (22) contains the component of effective potential in the form of a cross-term. It can be treated as a perturbation. Earlier, analogous procedures were carried out in 3D perfect metals for calculations of ground state energy $\varepsilon^{(0)}$ and effective masses m_{eff} of electrons by

Bardeen [48], Cohen and Ham [49] and for positrons by Stott and Kubica [50],

$$\varepsilon^{(1)} = \frac{\hbar^2 k^2}{2m_{\text{eff}}}.$$

In Refs. [48] and [49] the set of cellular wave functions was used. In Ref. [50] the function $\psi(\mathbf{r})$ was expanded in the set of plane waves in a crystal.

It turned out that the influence of vacancies on effective masses of electrons [36] and positrons [37] in melting point ($c_v \approx 10^{-3}$) is insignificant. In order to estimate the effective mass, we used in [36] the Bardeen approach [48] with s - and p -phase of scattering for $k = q_0$. For $c_v = 10^{-2}$ the calculated values of the electron effective mass $m_{\text{eff}} = 1.006, 1.01, 1.012$ and 1.014 for Na, Cu, Al and Pb, respectively. The small excess of m_{eff} over m indicates that the repulsion prevails over the attraction in the scattering of electrons by the supercell potential with the radius R_v .

C. c_v -expansions

We propose a method which combines two approaches. The first approach is based on a self-consistent solution for the monovacancy in 3D metal neglecting its surface. The second approach is based on a stabilized jellium model for uniform 3D metal with flat boundary, but the atom density of a metal is decreased due to the presence of vacancies superlattice of relative concentration c_v . In this case, the effective electron work function $W_{\text{eff},v}$ can be presented as a sum

$$W_{\text{eff},v} = W + \delta W_v^{\text{bulk}}, \quad (23)$$

where W is traditionally calculated by the density functional method a characteristic consisting of a volume component and a surface dipole barrier, and

$$\delta W_v^{\text{bulk}} = -\varepsilon^{(0)}. \quad (24)$$

For a semi-infinite metal [the x axis is perpendicular to the interface metal ($x \leq 0$) - vacuum ($x > 0$)] containing vacancies the equilibrium profile $n(x)$ satisfies the the Euler-Lagrange equation

$$\mu(x) = e\phi(x) + \langle \delta v \rangle_{\text{WS}} \theta(-x) + \frac{\delta G}{\delta n(x)} = \text{const}, \quad (25)$$

where the electrostatic potential $\phi(x)$ is determined by the integration of the Poisson equation

$$\frac{d^2 \phi}{dx^2} = -4\pi e[n(x) - \rho(x)], \quad \rho(x) = \bar{n}\theta(-x). \quad (26)$$

Here μ is the electron chemical potential; $\langle \delta v \rangle_{\text{WS}}$ is the stabilization potential, $\theta(-x)$ is the unit step function, $G[n]$ is the universal functional corresponding to ordinary jellium model with energy per electron $\varepsilon_J = \varepsilon_t + \varepsilon_{\text{xc}}$ (for

detail see Ref. [30]); distribution of the positive charge $\rho(\mathbf{r})$ is homogeneous inside the metal and zero outside it.

The condition $\mu(x) = \text{const}$ follows from the equivalence of the choice of the coordinate in (25). It is convenient to take $x = -\infty$, where the gradient terms (g. t.) vanish. Then the work function of the electrons can be found as

$$W = -\bar{\mu}. \quad (27)$$

Let us make a comparison between a defect-free half-infinity metal and a metal containing vacancies. The scenario for the formation of vacancies is not important in this context. It may be the Schottky mechanism or the ‘‘bubble blowing’’ mechanism [51]. It is important that the number of atoms in the sample is so large, that in the spaces between vacancies a density of atoms is the same as in perfect sample.

We average the charge density over the vacancy supercell. As a result, the electroneutrality condition in the bulk of a ‘‘fictitious, defect-free’’ metal is

$$\bar{n} = \bar{\rho} = \frac{Z\bar{n}_a}{1 + c_v}, \quad (28)$$

where Z is the valency of metal. The electron density satisfies the condition $\frac{4}{3}\pi r_s^3 \bar{n} = 1$; $r_s = r_0/Z^{1/3}$.

Carrying out the series expansion with respect to the small dimensionless parameter c_v in condition (28) and limiting ourselves to linear terms, we have

$$\bar{n} = \bar{n}^0 + \bar{n}^1 c_v, \quad \bar{n}^1 = -\bar{n}^0, \quad (29)$$

where \bar{n}^0 is the density of homogeneous electron gas for $c_v = 0$.

By analogy with the Refs. [42–44], in which a method is developed for determination of size corrections of energy characteristics of spherical clusters in the stabilized jellium (R^{-1} is a small dimension parameter), we represent characteristics of a metal containing vacancies as

$$\begin{aligned} n(x) &= n^0(x) + n^1(x)c_v + \dots, \\ \rho(x) &= \rho^0(x) + \rho^1(x)c_v + \dots, \\ \phi(x) &= \phi^0(x) + \phi^1(x)c_v + \dots, \\ \mu(x) &= \mu^0(x) + \mu^1(x)c_v + \dots \end{aligned} \quad (30)$$

This allows us to expand the equations (25) and (26) into series. Restricting ourselves to zero and first-order terms of expansion (superscripts ‘‘0’’ and ‘‘1’’, respectively), we have

$$\mu^0(x) = e\phi^0(x) + \frac{\partial g^0}{\partial n^0} + \langle \delta v \rangle_{\text{WS}}^0 \theta(-x) + \text{g. t.}, \quad (31)$$

$$\mu^1(x) = e\phi^1(x) + n^1(x) \frac{\partial^2 g^0}{\partial (n^0)^2} + \bar{n}^1 \frac{\partial \langle \delta v \rangle_{\text{WS}}^0}{\partial \bar{n}^0} \theta(-x) + \text{g. t.}, \quad (32)$$

$$\frac{d^2\phi^{0,1}(x)}{dx^2} = -4\pi e[n^{0,1}(x) - \rho^{0,1}(x)]. \quad (33)$$

In (32) $g^0 \equiv n^0(x)\varepsilon_J(n^0(x))$ is the energy density in LDA.

From condition $x = -\infty$, we have sum-rules

$$\bar{\mu}^0 = e\bar{\phi}^0(x) + \frac{\partial\bar{g}^0}{\partial\bar{n}^0} + \langle\delta v\rangle_{\text{WS}}^0 = -W^0, \quad (34)$$

$$\begin{aligned} \bar{\mu}^1 &= e\bar{\phi}^1 + \bar{n}^1 \frac{\partial^2\bar{g}^0}{\partial(\bar{n}^0)^2} + \bar{n}^1 \frac{\partial\langle\delta v\rangle_{\text{WS}}^0}{\partial\bar{n}^0} \\ &= e\bar{\phi}^1 + \bar{n}^1 [\bar{n}^0(\bar{\varepsilon}_{\text{SJ}}^0)'' + (\bar{\varepsilon}_{\text{J}}^0)'] = -W^1/c_v, \end{aligned} \quad (35)$$

where the energy per electron in the stabilized jellium $\varepsilon_{\text{SJ}} = \varepsilon_{\text{J}} + \bar{\varepsilon}$, $\bar{\varepsilon}$ is the electrostatic self-energy of the uniform negative in the Wigner-Seitz cell [30].

Note that $\bar{\mu}_0$ in Eq. (3) and $\bar{\mu}^0$ in Eq. (30) are the same, and $\bar{\mu}_1$ and $\bar{\mu}^1$ have different dimensions and are expressed in terms of characteristics of a defect-free metal with a flat surface.

Integration in Eq. (33) gives

$$\bar{\phi}^{0,1} = -4\pi e \int_{-\infty}^{\infty} dx x [n^{0,1}(x) - \rho^{0,1}(x)]. \quad (36)$$

Due to the fact that the vacancy shift of the electrostatic potential in the bulk $\bar{\phi}^1$ is only due to a decrease in average electron and ions densities in the metal, by analogy with self-compressed clusters [43, 44], where the effect is inversed, we have instead of (36)

$$\bar{\phi}^1 = \bar{n}^1(\bar{\phi}^0)'. \quad (37)$$

Here the primes denote derivatives with respect to \bar{n}^0 .

Using expression for the bulk modulus, $B^0 = (\bar{n}^0)^3(\bar{\varepsilon}_{\text{SJ}}^0)''$, the formulas (29) and (37), we finally have for first-order term

$$W^1 = -[e\bar{n}^0(\bar{\phi}^0)' + (B^0/\bar{n}^0 + \bar{n}^0(\bar{\varepsilon}_{\text{J}}^0)')] c_v. \quad (38)$$

As a result of this approach

$$W_{\text{eff},v} = W^0 + W_{\text{eff},v}^1, \quad (39)$$

and vacancy contribution

$$W_{\text{eff},v}^1 = W^1 + \delta W_v^{\text{bulk}}, \quad (40)$$

as a whole is expressed only through the characteristics of a defect-free metal. For defect-free Al and Na $W^0 = 4.30$ eV and 2.93 eV, respectively.

In the above exact formulas, the only $\bar{\phi}^0$ and $(\bar{\phi}^0)'$ terms require self-consistent calculations. Table II shows the values of the components formula (38). As we see, the contribution from the surface barrier $\sim (\bar{\phi}^0)'$ is very significant, competing with the bulk contribution in (38)

(a sum of terms in parentheses). In general, W^1 are negative in sign. In almost all cases, the major contribution of the effect is in the magnitude of δW_v^{bulk} in (40).

For Al at the melting point $c_v \approx 10^{-3}$. Consequently, the contribution of equilibrium bulk vacancies to the electron work function is approximately -0.2 eV. According to the paper [52], the concentration c_v should be much higher, then, respectively, the effect of vacancies will increase by many times.

Table II. The results (in eV) of the Kohn-Sham calculations for componets of formula (38) and vacancy contribution W_{eff}^1 (40) to the electron work function.

Metal	$e\bar{n}^0(\bar{\phi}^0)'$	B^0/\bar{n}^0	$\bar{n}^0(\bar{\varepsilon}_{\text{J}}^0)'$	W^1/c_v	$W_{\text{eff},v}^1/c_v$
Na	-0.773	1.77	0.0611	-1.07	-5.17
Al	-2.99	5.42	2.49	-4.92	-18.2

Small independent parameters R^{-1} and c_v appear, when applying these approaches to clusters.

D. Size vacancy contribution

Suppose that in large spherical clusters the potential field vacancy supercells has a ‘‘spherical periodicity’’ and function $\psi(\mathbf{r})$ in (11), which varies on the scale of the whole cluster, is modulated by the function $u(\mathbf{r})$. Then the boundary conditions for $\psi(\mathbf{r})$ on boundary lead to a discrete energy spectrum of electrons.

In the simplest case, assuming infinitely deep square well, the energy of the ground state of electrons in the potential well $v_{\text{eff}}(r)$ of the whole cluster was found in [53]. This approach uses the boundary condition

$$\psi(r)|_{r=R_{N,v}} = 0 \quad (41)$$

for Eq. (22) and allows to derive an analytical expression for vacancy quantum correction. The solution was obtained by expanding the function $\psi(\mathbf{r})$ in terms of the complete orthonormal set of eigenfunctions corresponding to the deep potential well. In this case, the term $\varepsilon^{(1)}$ in Eq. (12) can be written as

$$\varepsilon^{(1)} = \frac{\hbar^2\pi^2}{2mR_{N,v}^2} + \langle\delta V(r)\rangle_{R_{N,v}}. \quad (42)$$

The operator $\delta V(r)$ in (22) is used as a perturbation,

$$\delta V(r) = -\frac{\hbar^2}{m} \sum_{i=1}^{N_v} \frac{\nabla u_{\text{WS}}(\varrho)}{u_{\text{WS}}(\varrho)} \nabla. \quad (43)$$

The diagonal matrix element of the perturbation is the potential field $\delta V(r)$,

$$\langle\delta V\rangle_{R_{N,v}} = \int_{r < R_{N,v}} d\mathbf{r} \psi(r)\delta V(r)\psi(r), \quad (44)$$

averaged over the ground state with the quantum numbers $n_r = 1, l = 0$

$$\psi(r) = \frac{1}{\sqrt{4\pi}} \sqrt{\frac{2}{R_{N,v}}} \frac{\sin(\pi r/R_{N,v})}{r}. \quad (45)$$

As a result of the integration in Eq. (44) (see Appendix A), using (4), (7), (42) and (A11), the final expression of the ionization potential becomes

$$\begin{aligned} \text{IP}_{N,v} = & W_{\text{eff},v} + \frac{\alpha e^2}{N^{1/3}} \left(1 - \frac{1}{3}c_v\right) \\ & + \frac{1}{N^{2/3}} \left[-\tilde{\mu}_2 \left(1 - \frac{2}{3}c_v\right) \right. \\ & \left. - \frac{\hbar^2 \pi^2}{2mr_0^2} \left(1 - \frac{2}{3}c_v - D_1 \frac{L_v}{r_0} c_v^{1/3}\right) \right], \quad (46) \end{aligned}$$

where $D_1 \approx 2.7$. Here we neglected the size dependence in δW_v^{bulk} and the vacancy dependence in $\tilde{\mu}_1$ and $\tilde{\mu}_2$. In our work [53] we used δW_v^{bulk} instead of $W_{\text{eff},v}$.

The corresponding expression for electron affinity $\text{EA}_{N,v}$ is obtained from (46) by replacing $\alpha \rightarrow -\beta$.

In deriving $\varepsilon^{(1)}$, we used the boundary condition (41). It does not take into account electron spillover. The simplest way to account for the spillover is to use perturbation theory [54], taking into account the finite depth of the spherical well $\approx \bar{v}_{\text{eff}}$, $\bar{v}_{\text{eff}} = -6$ and -16 eV for Na and Al, respectively (Fig.1). There is no analytical solution for a spherical well, and for a cluster-cube the result is known [55]. This means that that result $\sim \hbar^2$ in Eq. (46) for hard wall-cube must be multiplied by

$$\left(1 - \frac{4}{R_N k_0} + O(R_N^{-2})\right),$$

where $k_0 = \sqrt{-2m\bar{v}_{\text{eff}}}$. The account of the spillover will result in the appearance the term $-A/N^{1/3}$ in the last parenthesis in the (46), where $A \approx 1$ for Na and Al. Thus it is obvious that in the derivation of the term we neglected the terms proportional $1/N$.

Therefore, taking into account that $c_v \ll 1$, condition (41) limits the value of c_v from below. As a result of the electron spillover neglect, the applicability of formula (46) is possible under the condition

$$1/N \ll c_v = N_v/N \ll 1. \quad (47)$$

The lower size limit where the concepts of supercells work is two supercells shells ($N_v \geq 55$). The use of this technique for one supercells shells ($N_v = 13$) is already an extrapolation.

The straightforward application of inequality (6) and the boundary condition (41) in the paper [53] leads to the erroneous application of formula for $\text{IP}_{N,v}$ to the case of a monovacancy in a cluster (see Fig. 3 in [53]). The perturbation theory made it possible to introduce more realistic description of the cluster. Because of this, without changing the form of (A11), the limits of applicability

(47) of the theory for a dilute subsystem of vacancies in a cluster are formulated in the case of a discrete electron spectrum.

For $c_v = 0.01$ and the first two coordination spheres of supercells, the total number of atoms in the cluster is $N = 1300$ and 5500 , which corresponds to $R_{N,v} \approx 1.8$ and 2.9 nm for Al, respectively.

However, the choice of the applicability criteria of (46) is more consistent from the condition of expansion of the electron chemical potential in power series of the inverse radius ($c_v = 0$)

$$\tilde{\mu}_1 N^{1/3} \geq \tilde{\mu}_2 + \frac{\hbar^2 \pi^2}{2mr_0^2}. \quad (48)$$

In its turn, this leads to the values $N \geq 9.68 \cdot 10^3$ ($R \approx 4.5$ nm) and $N \geq 5.45 \cdot 10^4$ ($R \approx 6$ nm) for Na and Al, respectively.

The large clusters are detectable in the experiment. For example, [56] reported on a photoelectron spectroscopy and determination of the steps of the Coulomb staircase ($E_C = e^2/R_N$) of ionized clusters $\text{Al}_{N \leq 32000}^-$ with an accuracy of approximately 10^{-2} eV.

The value of δ_1 in (4) was determined repeatedly [51]. We use calculated within a stabilized jellium model values $\delta_1 = \sigma_1/\sigma_0 = 0.32r_0, 0.57r_0$ for Na and Al, respectively [$\sigma_1 = \gamma/2$ in Table VI of work [33]]. The experimental values of $W_0 = 2.75$ eV, $\text{IP}_1 = 5.14$ eV, $\sigma_0/B_0 = 0.70 a_0$ for Na and $W_0 = 4.28$ eV, $\text{IP}_1 = 5.99$ eV, $\sigma_0/B_0 = 0.40 a_0$ for Al are taken from [57].

In Fig. 2 the dependences (9) and (46) are shown for Na and Al. Due to the fact that the formula (9) gives the value IP_1 only 10% higher than the experimental one, and the experimental values of W_0 for a number of materials are strongly dependent on measurement techniques, it was assumed from measurements $\text{IP}_{N \leq 100}$ for magic numbers (see Fig. 28 in [23]) using (9) to determine the true values W_0 . On the other hand, the the last term in (46) that is conditioned by quantization lead to non-linear behavior of $\text{IP}(N^{-1/3})$ and $\text{EA}(N^{-1/3})$ in the region of small N .

The presented analytical approach seems to be promising for experimental estimation of the concentrations of point defects or impurities in metal clusters. To this end, it is first needed to calculate the scattering length of electrons on the corresponding defect in 3D metal. In particular, the problem of vacancies concentration in the cluster at the melting point can be solved. Using Fig. 2 as grid of values, if the experimental value of $\text{IP}_{N,v}$ resides at one of the curves, the value $c_v(N)$ is fixed for a given temperature.

E. Small clusters containing monovacancy

For simplicity, the density of the positive charge background of defected and perfect (free-defect) clusters is

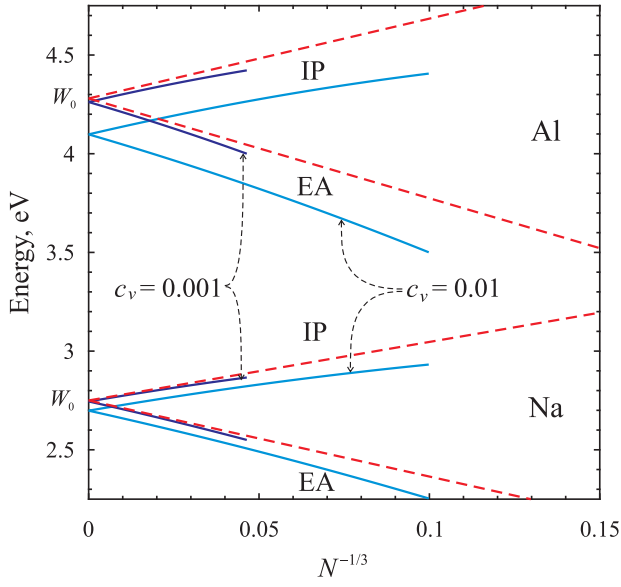


Figure 2: The calculated dependences $IP_{N,v}$ and $EA_{N,v}$ for large clusters of Na and Al by the formulas: (46) – solid lines ($c_v = 0.001$ and 0.01) under the condition (47) and (9) – red dashed lines.

chosen in the form

$$\rho_v(r) = \bar{n}\theta(r - r_0)\theta(R_{N,v} - r) \quad (49)$$

and

$$\rho(r) = \bar{n}\theta(R_N - r), \quad (50)$$

respectively.

Wave functions and eigenvalues of energies $\varepsilon_{j,v}$ are the solution of the Kohn-Sham equations with effective single-electron potential, including electrostatic and exchange-correlation potential in the LDA. The energy is measured from the vacuum level, that is, on the energy of an electron with zero kinetic energy, located far from the sample ($r \gg R_{N,v}$).

The electrostatic potential is a solution of the Poisson equation for a fixed condition

$$\int_0^\infty dr 4\pi r^2 [\rho_v(r) - n_v(r)] = Q/e, \quad (51)$$

where Q is the total charge of the cluster.

Fig. 3 shows the profiles of the electron distribution and effective potential for a defect-free cluster and cluster with vacancy, containing the same number of atoms $N = 12$. The vacancy radii for Na and Al clusters are shown in the figure. Their radii differ according to the definition (5). The insets show the tails of electron profiles and the potentials far from clusters. Despite the fact that electronic distributions are rapidly decreasing functions of radial distance r , the potential tails extend far (the calculation was carried out to $r \approx R_N + 900 a_0$). For charged clusters, the electrostatic potential decreases

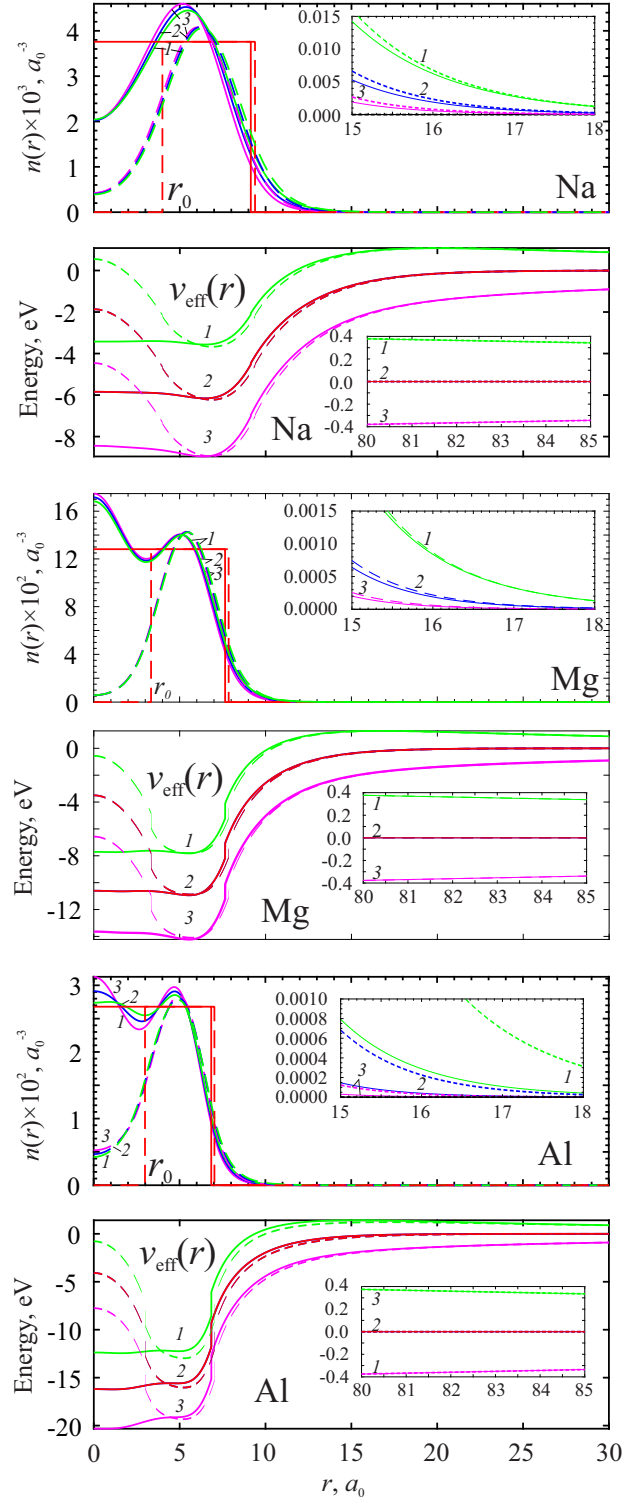


Figure 3: Self-consistent profiles of spatial distribution of electrons and effective potential for a charged and neutral perfect clusters (solid lines), and a cluster with a monovacancy (dashed lines) containing the same number of atoms $N = 12$; 1 – $Q = -e$, 2 – $Q = 0$, 3 – $Q = +e$.

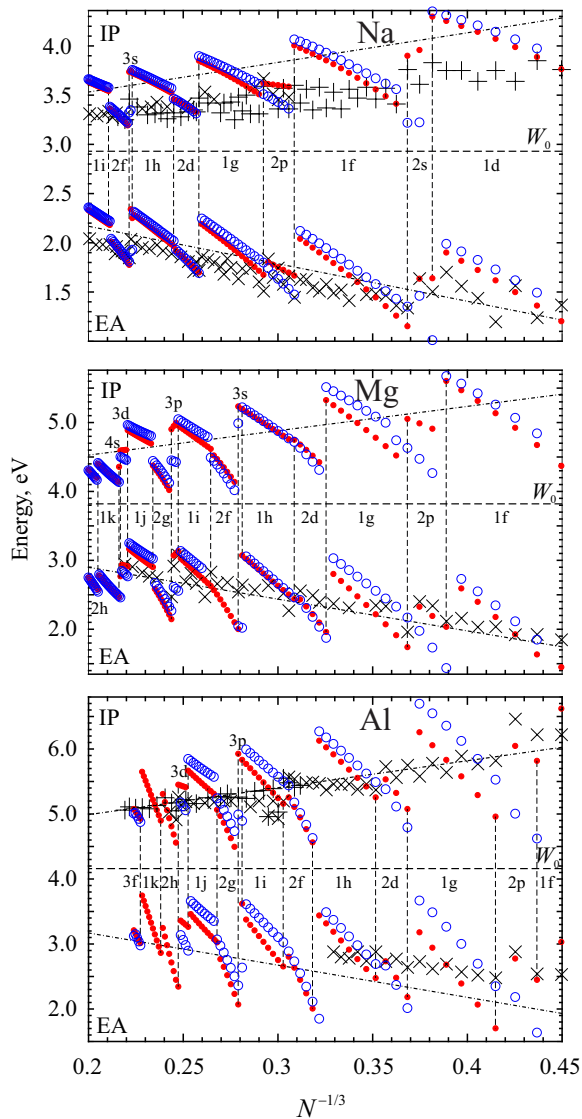


Figure 4: The ionization potential IP and the electron affinity EA, calculated from the formulas (2) for perfect clusters (filled red points) and clusters with monovacancy (open blue circles). Experimental values: Na (+) [23], (x) [58], Mg (x) [58], and Al (+) [22], (x) [23]. Dash-dotted lines are the asymptotics (52). The letters s, p, d, f, g, h, i, j, k, l correspond to the quantum orbital numbers $l = 0, \dots, 9$.

asymptotically beyond $\sim Q/r$. It is interesting to compare the profiles of electrons and potentials in Fig. 3 for Na_{12} and Al_{12} with analogous profiles for 3D metals in Fig. 1. For large clusters, the spatial profile becomes similar to the profile near the surface of a semi-infinite metal, containing a large number of the Friedel oscillations. Obtained profiles allow us to calculate the total energy of the cluster $E_{N,v}^{\pm}$ (and E_N^{\pm}).

Fig. 4 shows the results of direct calculations of IP and EA by the formula (2), as well as the asymptotics (9). A difference between perfect clusters and defective clusters

can be understood from this figure as well as from Tables III and IV. For Na with the increase of N , starting from 12, this difference can be 0.1 – 0.5 eV (for Mg and Al about twice as much). Maximum difference is observed at the transition from a completely filled shell to an empty one. As N increases, this difference is leveled. For clarity, the results of the calculations are given in coordinates $N^{-1/3}$. For clusters with a monovacancy $c_v = 1/N$, therefore there is a correspondence $N^{-1/3} = c_v^{1/3}$. In our case $c_v \rightarrow 0$ for $N \rightarrow \infty$. If the vacancy is not single, but their concentration is low (vacancies do not interact with each other), according to our results, it is possible to track the dependence of energy characteristics on the concentration of vacancies.

The ionization potential and the electron affinity show a strong oscillatory behavior due to the spherical shell structure. They tend to W_0 asymptotically slow enough, due to high orbital degeneracy and large angular quantum numbers l . According to the results of experiments, the oscillations should be much weaker. Going beyond LDA and using local spin density approximation (LSDA) allows to reduce oscillations [59].

Using the Koopmans' theorem, the formulas (2) can be rewritten [60, 61] in form

$$\begin{aligned} \text{IP}_{N,v} &= -\varepsilon_{N,v}^{\text{HO}} + \frac{e^2}{2C_{N,v}^+}, \\ \text{EA}_{N,v} &= -\varepsilon_{N,v}^{\text{LU}} - \frac{e^2}{2C_{N,v}^-}, \end{aligned} \quad (52)$$

where $\varepsilon_{N,v}^{\text{HO}} / \varepsilon_{N,v}^{\text{LU}}$ and $C_{N,v}^{\pm}$ are the energy of the upper occupied / lower unoccupied orbital and electrical capacitances, respectively.

The spectra for perfect Na and Al clusters, shown in Fig. 5 demonstrate the filling of electronic shells as the number of electrons is increased. For partially filled shells $\varepsilon_{N,v}^{\text{HO}} = \varepsilon_{N,v}^{\text{LU}} \approx \mu(R_{N,v})$. The maximum values of $\varepsilon_{N,v}^{\text{HO}}$ correspond to completely filled shells, and magic numbers of atoms N^* for spherical perfect clusters and clusters with vacancy does not coincide in all cases. For Na the obtained values are $N^* = 2, 8, 18, 20, 34, 40, 58, 68, 90, 92, 106, 132, 138, 168, 186, 196, 198, (230), 232, (252), 254$; for Mg $N^* = 1, 4, 9, 10, 17, 20, 29, 34, 45, 46, 53, 66, 69, 78, 93, 98, (99), \{115\}, (116), \{126\}, 127, 134, 153, 156, 169, 178, 199, 204, 219$; for Al $N^* = 6, (30), 44, 46, 52, 62, \{66\}, (84), (102), \{104\}, \{136\}, 146, \{154\}, (180), (202), 204$. In round brackets, the obtained values are given for defective clusters which do not coincide with the corresponding values for perfect clusters, and in braces – on the contrary.

As $R_{N,v}$ increases, the values $\varepsilon_{N,v}^{\text{HO}}$ and $\varepsilon_{N,v}^{\text{LU}}$ oscillate and tend to $\mu(R_{N,v})$ for $R \rightarrow \infty$. Amplitude of oscillations decreases approximately as $R_{N,v}^{-3}$.

Let us denote the difference

$$\Delta(\text{IP}_N) = \text{IP}_{N,v} - \text{IP}_N.$$

and return to Fig. 4. At first sight, the sign $\Delta(\text{IP}_N) > 0$ is unexpected (circles are placed above the points for

the same N). Exceptions are clusters with such N that maximum contribution is given by levels with low l (s , p - and partially d -orbital). In Fig. 4 these narrow areas are enclosed between vertical dashed lines.

Table III. Computed quantities IP and EA (in eV) for Na clusters. Experimental values of IP_{exp} (Na_{17-94} - [23], $\text{Na}_{132-140}$ - [58]) and EA_{exp} (Na_{17-196} - [58]).

N	IP_N	$\text{IP}_{N,v}$	IP_{exp}	EA_N	$\text{EA}_{N,v}$	EA_{exp}
17	4.25	4.31	3.75	1.90	1.99	1.70
18	4.30	4.35	3.83	1.64	1.01	1.50
19	3.96	3.22	3.61	1.63	1.46	1.64
20	3.90	3.22	3.76	1.15	1.35	1.34
21	3.41	3.35	3.41	1.26	1.43	1.36
22	3.49	3.46	3.57	1.35	1.40	1.46
33	3.98	4.04	3.42	2.04	2.12	1.63
34	4.00	4.06	3.60	1.66	1.47	1.45
35	3.58	3.36	3.36	1.69	1.53	1.66
36	3.59	3.40	3.57	1.72	1.58	1.58
39	3.61	3.48	3.57	1.80	1.74	1.84
46	3.64	3.71	3.48	1.89	1.98	1.63
47	3.66	3.73	3.25	1.93	2.01	1.79
48	3.68	3.75	3.43	1.96	2.04	1.75
49	3.70	3.77	3.37	1.99	2.06	1.84
57	3.83	3.88	3.44	2.19	2.24	1.86
58	3.85	3.89	3.47	1.70	1.69	1.72
59	3.33	3.31	3.33	1.72	1.72	1.81
90	3.75	3.75	3.39	2.25	1.93	2.01
91	3.75	3.34	3.40	2.34	1.91	2.03
92	3.73	3.32	3.46	1.77	1.81	1.85
93	3.19	3.22	3.29	1.79	1.83	1.87
94	3.20	3.23	3.25	1.81	1.85	1.89
131	3.66	3.69	—	2.37	2.40	—
132	3.67	3.69	3.33	2.33	2.18	2.08
133	3.62	3.46	—	2.32	2.17	—
134	3.60	3.45	—	2.31	2.17	2.18
137	3.56	3.43	3.41	2.27	2.16	2.17
138	3.54	3.43	3.46	1.91	1.95	1.96
139	3.19	3.23	—	1.92	1.96	—
140	3.20	3.23	3.21	1.93	1.97	1.99
195	3.47	3.47	—	2.26	2.25	2.14
196	3.47	3.47	—	2.17	2.15	2.16
197	3.39	3.38	—	1.99	2.16	—
252	3.72	3.72	—	2.50	2.44	—
253	3.73	3.67	—	2.50	2.42	—
254	3.73	3.64	—	2.24	2.24	—
255	3.46	3.47	—	2.24	2.25	—
256	3.47	3.47	—	2.24	2.25	—
257	3.47	3.48	—	2.24	2.25	—
258	3.48	3.48	—	2.25	2.25	—

From an analysis of the asymptotic behavior of IP_N and $\text{IP}_{N,v}$ the basic vacancy dependence is contained in the work function $W_{\text{eff},v} < W_0$ (see (39) and Table II).

In the case of small defected clusters, the perturbation of the vacancy becomes essential, provided concentration $c_v \sim R_N^{-3}$. It follows from Fig. 3 that the behavior of $v_{\text{eff},v}(r)$ is such that the electrons are squeezed out by a

vacancy from the center of the cluster to its surface and are grouped, mainly, in the spherical layer $r_0 < r < R_N$. And when integrating in spherical coordinates, the expression for the total energy gives the main contribution to the energy. This is confirmed by the spectral values of the energies, corresponding to the points (circles) in Fig. 5. As an example, we give the values $\varepsilon_{n_r,l}$ (n_r and l are the radial and orbital quantum numbers) for perfect and defective (in parentheses) clusters: $\varepsilon_{0,0} = -4.925$ (-4.577), $\varepsilon_{0,1} = -3.871$ (-3.831), $\varepsilon_{0,2}^{\text{HO,LU}} = -2.595$ (-2.708) eV for Na_{12} ; and $\varepsilon_{0,0} = -5.073$ (-4.755), $\varepsilon_{0,1} = -4.177$ (-4.135), $\varepsilon_{0,2}^{\text{HO}} = -3.119$ (-3.189), $\varepsilon_{1,0}^{\text{LU}} = -2.787$ (-2.048) eV for Na_{18} .

Table IV. Computed quantities IP and EA (in eV) for Al clusters. Experimental values of IP_{exp} (Al_{20-63} - [23], $\text{Al}_{89,90}$ - [22]) and EA_{exp} (Al_{20-23} - [23]).

N	IP_N	$\text{IP}_{N,v}$	IP_{exp}	EA_N	$\text{EA}_{N,v}$	EA_{exp}
20	5.07	4.79	5.75	2.18	2.01	2.64
21	5.32	5.11	5.56	2.48	2.37	2.77
22	5.53	5.38	5.73	2.73	2.66	2.73
23	5.25	5.49	5.37	2.47	2.69	2.88
29	6.02	6.17	5.37	3.31	3.49	—
30	6.12	6.27	5.47	3.43	1.85	—
31	4.56	4.63	5.49	2.00	2.11	—
32	4.76	4.83	5.48	2.24	2.34	—
35	5.25	5.22	5.57	2.80	1.83	—
36	5.15	5.30	5.20	2.65	2.13	—
48	4.62	4.85	5.20	2.38	2.63	—
59	5.55	5.75	5.13	3.36	3.58	—
60	5.59	5.78	5.16	3.41	3.62	—
61	5.62	5.81	5.10	3.46	3.66	—
62	5.66	5.84	5.15	3.26	2.89	—
63	5.41	5.05	5.19	3.29	2.98	—
89	5.07	5.00	5.07	3.21	3.12	—
90	4.73	4.71	5.08	2.87	2.82	—
111	5.51	5.26	—	3.75	3.52	—
112	5.53	5.24	—	3.79	3.51	—
113	4.63	4.69	—	2.91	2.99	—
114	4.67	4.74	—	2.96	3.04	—
170	5.10	5.14	—	3.75	3.81	—
171	5.13	5.16	—	3.79	3.84	—
213	5.54	5.62	—	4.56	4.67	—
214	5.57	5.65	—	4.60	4.70	—
225	5.90	5.95	—	5.00	5.11	—
226	5.81	5.81	—	4.93	5.00	—
227	5.82	5.83	—	4.97	5.04	—
230	5.86	5.86	—	5.08	5.14	—
231	5.86	5.87	—	5.11	5.17	—
263	6.44	6.36	—	6.06	6.01	—

With increasing N , the contribution from the cluster bulk becomes more and more important and for large enough N the point and the circles are interchanged, that is, the difference $\Delta(\text{IP}_{N \rightarrow \infty})$ becomes negative by the sign.

Self-consistent values of IP, EA, ε^{HO} and ε^{LU} , which

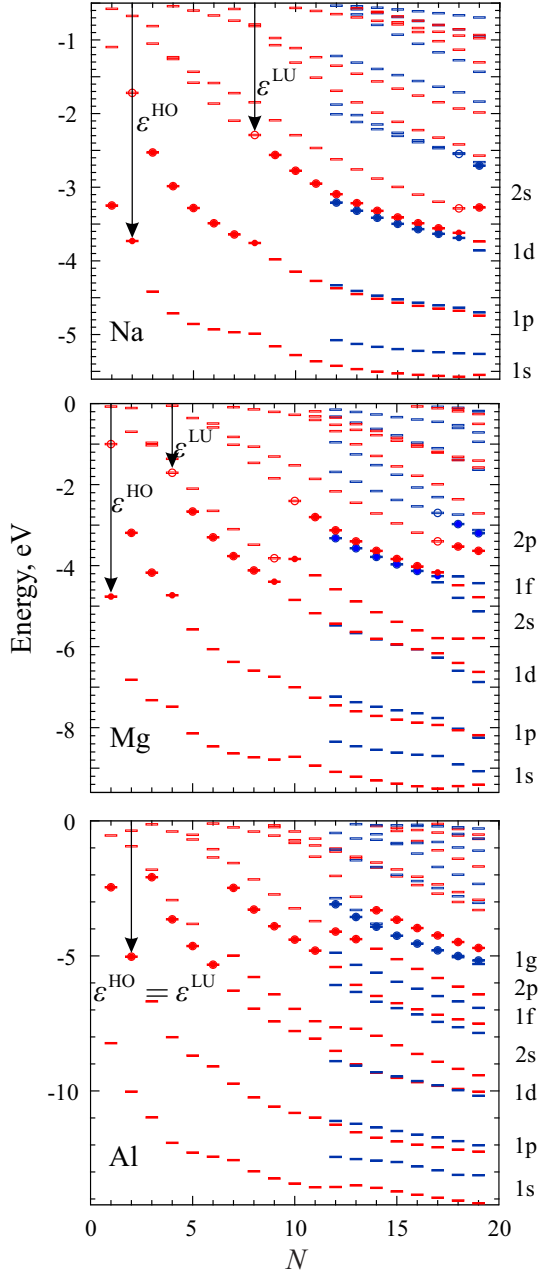


Figure 5: Kohn-Sham one-electron eigenvalues for perfect (in red) and defected (in blue) clusters. The long solid and open rectangles correspond to occupied and unoccupied levels, respectively. The upper occupied $\varepsilon_N^{\text{HO}}$ (filled red and blue points) and lower unoccupied $\varepsilon_N^{\text{LU}}$ (open red and blue circles) energy levels are marked.

are found according to the general formulas (2), allow us to evaluate capacitances of charged and neutral clusters using the expressions (52)

$$C_{N,v}^+ = \frac{e^2}{2(\text{IP}_{N,v} + \varepsilon_{N,v}^{\text{HO}})}, \quad C_{N,v}^- = \frac{-e^2}{2(\text{EA}_{N,v} + \varepsilon_{N,v}^{\text{LU}})},$$

$$C_{N,v} = \frac{e^2}{\text{IP}_{N,v} + \varepsilon_{N,v}^{\text{HO}} - \text{EA}_{N,v} - \varepsilon_{N,v}^{\text{LU}}}. \quad (53)$$

Similar formulas for C_N correspond to a defect-free clusters.

In classical electrostatics, the capacitance of conducting sphere is determined by its radii $R_{N,v}$. Surface roughness on an atomic scale (atoms have a finite volume) does not allow to determine exactly the boundary [51, 62]. In the jellium, the boundary of the ion core always corresponds to the coordinate $r = R_{N,v}$. However, the electronic cloud is more and more “splashes out” beyond the boundary of the core as its radius $R_{N,v}$ decreases. Moreover, such a “splashing” depends on the sign of the excess cluster charge (Fig. 3). As a result, the quantities $C_{N,v}^+$, $C_{N,v}^-$ and $C_{N,v}$ are equal to each other only in the limit $N \rightarrow \infty$.

Fig. 6 shows the results of calculations for capacitances C_N and $C_{N,v}$ normalized by their radius R_N and $R_{N,v}$ (atomic units), respectively. Sign-alternating difference

$$\Delta\tilde{C}_N^\pm \equiv \frac{C_{N,v}^\pm}{R_{N,v}} - \frac{C_N^\pm}{R_N}$$

is observed for certain intervals of N , which correspond to filling of s - and p - electronic shells. The difference $\Delta\tilde{C}_N$ is determined mainly by the ratio of the quantities ε^{HO} and ε^{LU} for different l in perfect and defective clusters, which can vary depending on the radial quantum number. The capacitance of defective clusters at filling shells with small l is larger than for perfect ones, and the opposite relation is observed for large l .

Using the experimental values of IP_1 and EA_1 for the Na atom ($R_1 = r_0$), and also the condition $\varepsilon_1^{\text{HO}} = \varepsilon_1^{\text{LU}}$ for unfilled shells, as a test, we get the value $C_1/r_0 = 1.8$. It is in a satisfactory agreement with the calculated values for the smallest clusters. For non-closed electronic shells, the cluster may have a lower symmetry (spheroidal or triaxially deformed droplet [25]).

The charging effect expressed in the electric capacitance of the cluster anions and cations depends on the sign of the excess charge. Normalization of the capacitance allows to give a simple interpretation of the results of calculations: an excess negative charge leads to an effective increase in the electron cloud (effective radius) of the cluster, and excess positive charge results in a decrease of both effective radius and capacitance. This is qualitatively confirmed by the behavior of electronic profiles in Fig. 3.

In [63], in addition to measurements of thermal capacity of cluster anions and cations Al_{35-70} , the ionization potentials and electron affinity were calculated. Calculations are carried out by the DFT under the condition of a global minimum of the total energy for various configurations of atoms. The results (in eV) presented in Fig. 9 in [63] are approximated by us in the form

$$\text{IP}_N = 4.17 + 3.97/N^{1/3}, \quad (54)$$

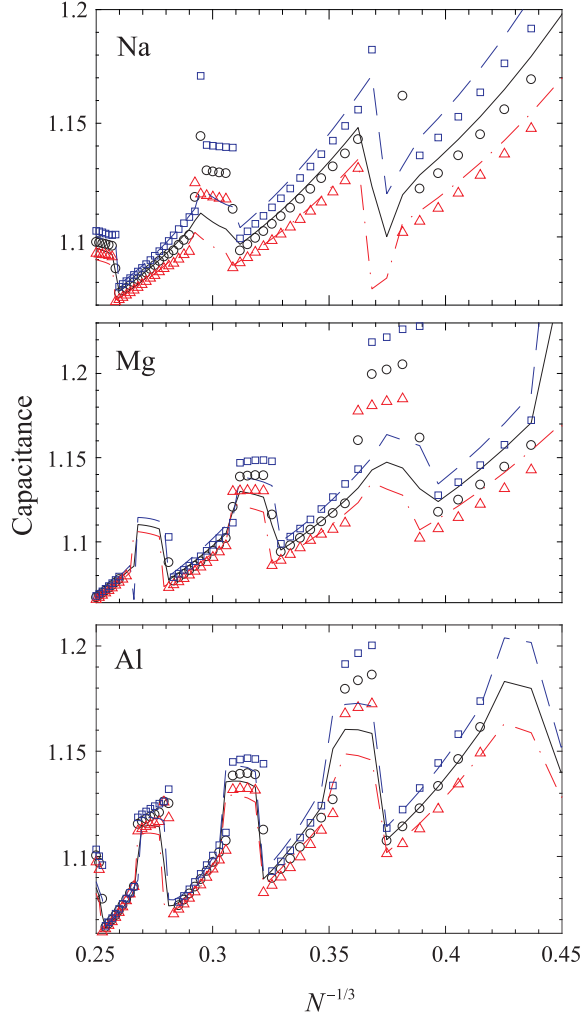


Figure 6: The results of calculations by formulas (53) for normalized capacitances of the perfect clusters (red dash-dotted, black solid and blue dashed lines correspond to positively charged, neutral, and negatively charged clusters, respectively) and clusters with a monovacancy (red triangles, black open circles, and blue open square, respectively).

$$EA_N = 3.88 - 3.05/N^{1/3}. \quad (55)$$

It follows from (9) that IP_N and EA_N must approach the same quantity W_0 with increase of N . Such a tendency does not agree with (54) and (55). Also the comparison of (54) and (55) from one side and (9) from another side allows to extract values of $\tilde{\mu}_1$. The results are ambiguous: it follows from (54) that $\tilde{\mu}_1 \approx +0.58$ eV, while $\tilde{\mu}_1 \approx -1.51$ eV from (55). Let us remind that $\tilde{\mu}_1 \approx +0.68$ eV for Na [35, 40].

III. DISSOCIATION AND COHESION ENERGIES

The dissociation energy of a neutral metallic (Me) cluster according to the reaction $Me_N \rightarrow Me_{N-1} + Me_{at}$ is

determined by the difference in total energies

$$\varepsilon_N^{\text{dis}} = [E_{N-1} + E_{at}] - E_N = N\varepsilon_N^{\text{coh}} - (N-1)\varepsilon_{N-1}^{\text{coh}}. \quad (56)$$

In the stabilized jellium, the energy of the atom E_{at} is the total energy of a metal sphere of radius r_0 .

By definition, the cohesive energy $\varepsilon_N^{\text{coh}}$ is the binding energy (atoms in the cluster) per atom. It is determined by the difference in the total energy of the N free atoms and the energy of a cluster consisting of N atoms

$$\varepsilon_N^{\text{coh}} = (NE_{at} - E_N)/N = E_{at} - E_N/N. \quad (57)$$

For $N \rightarrow \infty$, $\varepsilon_N^{\text{coh}} \rightarrow \varepsilon_\infty^{\text{coh}} \equiv \varepsilon^{\text{coh}}(r_0)$. The calculated values of $\varepsilon^{\text{coh}}(r_0) = 1.16, 1.17$ and 3.97 eV, respectively for Na, Mg and Al, are in satisfactory agreement with the experimental values of $\varepsilon_\infty^{\text{coh}} = 1.11, 1.51$ and 3.39 eV (see Ref. [33] and references therein).

The binding equation has the form

$$\varepsilon_N^{\text{coh}} = \frac{1}{N} \sum_{n=2}^N \varepsilon_n^{\text{dis}}. \quad (58)$$

Asymptotics of the size dependence of the cohesion energy (57) is well known [1]

$$\varepsilon_N^{\text{coh}} = \varepsilon^{\text{coh}}(r_0) - \frac{2\sigma_0}{n_{at}R_N}, \quad (59)$$

where the last term can be written as $-Z\mu_1/R_N$.

It should be noted that even in the works of Frenkel and Langmuir it is noted that for some substances at low temperatures a universal ratio is observed

$$\frac{4\pi r_0^2 \sigma}{q} \approx \frac{2}{3},$$

which is constructed from the observed values: the average distance between atoms r_0 , the surface energy σ , and the heat evaporation $q = \varepsilon^{\text{coh}}(r_0)$ (see Table 2 in [51]). Using this relation, the asymptotics (59) can be rewritten in a form convenient for estimations

$$\varepsilon_N^{\text{coh}} \approx \varepsilon^{\text{coh}}(r_0) \left(1 - \frac{4}{9N^{1/3}}\right).$$

Next, using Eqs. (59) and (56), we find a coincidence of the asymptotics $\varepsilon_N^{\text{coh}}$ (59) and $\varepsilon_N^{\text{dis}}$.

It is of interest to determine the effect of charging on dissociation and cohesion energies of clusters. The previous results in electronic model and molecular dynamics simulations show that fragmentation consists mainly in emission of single atoms [64]. Due to the fact that the ion work function is greater than the heat of evaporation of the neutral atom [55], using Eqs. (56), (57) and expressions

$$\begin{aligned} \varepsilon_N^{\text{dis},\pm} &= N\varepsilon_N^{\text{coh},\pm} - (N-1)\varepsilon_{N-1}^{\text{coh},\pm}, \\ \varepsilon_N^{\text{coh},\pm} &= E_{at} - E_N^\pm/N, \end{aligned} \quad (60)$$

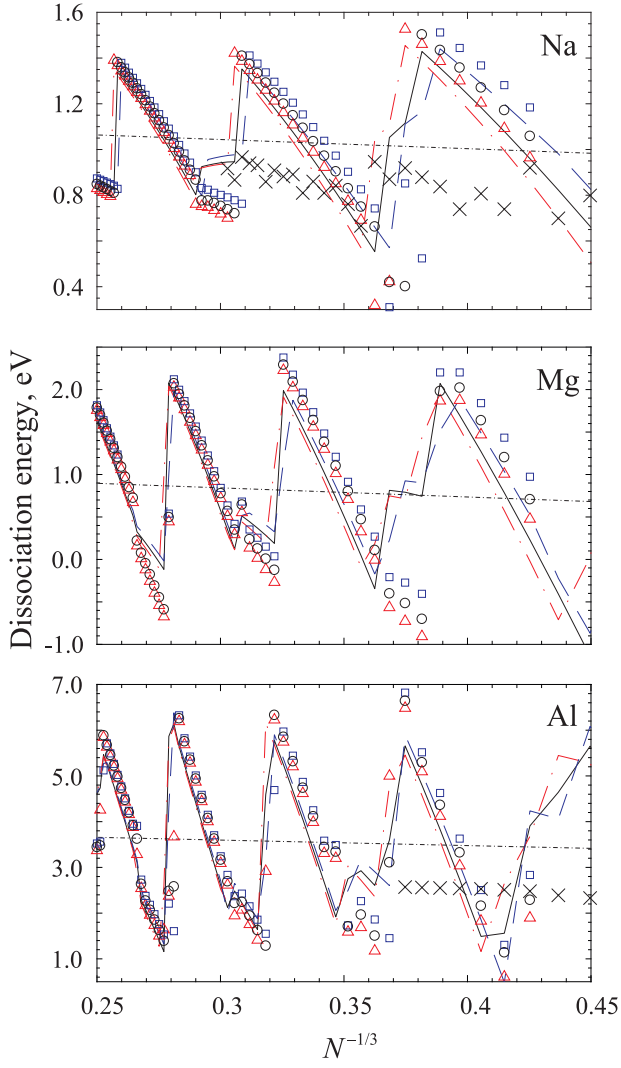


Figure 7: The calculated dissociation energy $\varepsilon_N^{\text{dis}}$ of the perfect clusters (red dash-dotted, black solid and blue dashed lines correspond to positively charged, neutral, and negatively charged clusters, respectively) and clusters with a monovacancy (red triangles, black open circles, and blue open square, respectively); experimental (\times) values [21]; black dash-dotted lines are asymptotics (59).

the energy differences can be expressed as

$$\begin{aligned} \Delta\varepsilon_N^{\text{dis},+} &\equiv \varepsilon_N^{\text{dis},+} - \varepsilon_N^{\text{dis}} = \text{IP}_{N-1} - \text{IP}_N, \\ \Delta\varepsilon_N^{\text{dis},-} &= \text{EA}_N - \text{EA}_{N-1}, \\ \Delta\varepsilon_N^{\text{coh},+} &= -\frac{1}{N}\text{IP}_N, \quad \Delta\varepsilon_N^{\text{coh},-} = \frac{1}{N}\text{EA}_N. \end{aligned} \quad (61)$$

Figs. 7 and 8 show the dissociation and cohesion energies of perfect clusters and clusters containing monovacancy. Size dependence of the dissociation energy in Fig. 7 is represented by quantum oscillations around the asymptotical dependence. The values $\varepsilon_{N,v}^{\text{dis}}$ for defective cluster, with large l , are larger than for a perfect one, and for small l , they interchange. For perfect and defective clusters, in addition to a change of order filling of

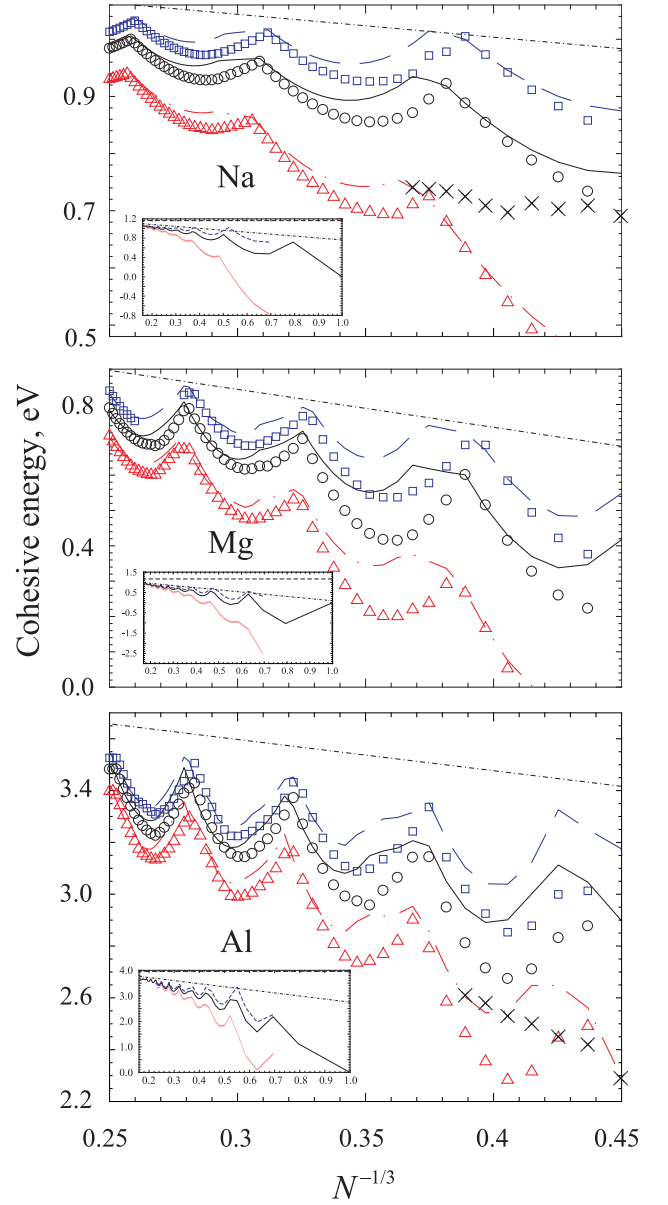


Figure 8: Computed quantities $\varepsilon_N^{\text{coh}}$ (red dash-dotted, black solid and blue dashed lines correspond to positively charged, neutral, and negatively charged clusters, respectively) and clusters with a monovacancy (red triangles, black open circles, and blue open square, respectively); experimental (\times) value [21]; black dash-dotted lines – asymptotics (59). The insets give the results for perfect clusters in the whole range of N under the study.

electronic levels, a significant difference in the behavior of dissociation energy with the same number of atoms N is also seen: for small l , dissociation energy of perfect clusters decreases with increasing N , while it increases for defective clusters. Comparison of the data in Fig. 8 and 9 confirms the accuracy of formula (58), and also explains the difference in the position of local maxima. The calculated values of $\varepsilon_{N,v}^{\text{coh}}$ are closer to the experimen-

tal values, obtained for $T = 150$ K [21], than $\varepsilon_N^{\text{coh}}$. We note that near the phase transition the quantities $\varepsilon_N^{\text{dis}}$, extracted from measurements of melting temperature and latent heat of the transition can be negative [18].

Thus, we can conclude that the most stable defect-free clusters are those, which have latest filled levels with a small l , and for defective one - on the contrary. In the experiments, the size oscillations $\varepsilon_N^{\text{dis}}$, are apparently suppressed by temperature effects (see Fig. 9 in [20]).

As shown in Fig. 8 cohesion energy of cluster anions and cations is different from neutral clusters. Excess positive charge leads to a decrease in the energy of cohesion due to the increase of the forces of electrostatic repulsion, while excess negative charge leads to the opposite effect. A behavior of dissociation and cohesion energies of charged clusters is described by the Eq. (61).

IV. MONOVACANCY-FORMATION ENERGY

A considerable number of papers deal with first principles (*ab initio*) calculations of the monovacancy-formation energies in metals [65]. In the stabilized jellium and the liquid drop models the energy of cohesion of an atom and the monovacancy-formation energies are investigated in form of the Padé expansion [33] (see also [51]). Within the notation of the work [51], the results of [33] can be expressed as

$$\begin{aligned}\varepsilon^{\text{coh}}(r_0) &= 4\pi r_0^2 \sigma_0 \left(1 + \tilde{\delta}_1 + \tilde{\delta}_2\right), \\ \varepsilon^{\text{vac}}(r_0) &= 4\pi r_0^2 \sigma_0 \left(1 - \tilde{\delta}_1 + \tilde{\delta}_2\right),\end{aligned}\quad (62)$$

where $\tilde{\delta}_1 \equiv \delta_1/r_0$ and $\tilde{\delta}_2 \equiv \delta_2/r_0^2$.

Calculated in [37] $\varepsilon_\infty^{\text{vac}} \equiv \varepsilon^{\text{vac}}(r_0) = 0.33, 0.72$ and 1.00 eV agree with the experimental values of 0.335, 0.84 and 0.73 eV for Na, Mg and Al, respectively [66].

Using values $\varepsilon^{\text{coh}}(r_0)$ and $\varepsilon^{\text{vac}}(r_0)$, and $\tilde{\delta}_2 = -0.13$ (Na), -0.015 (Mg) and $+0.22$ (Al) from [33], we find $\tilde{\delta}_1 = 0.32$ (Na), 0.54 (Mg) and 0.57 (Al). The values δ_1 and δ_2 are necessary for us in order to construct the asymptotics of the monovacancy-formation energies.

For clusters, self-consistent calculations of $\varepsilon_{N,v}^{\text{vac}}$ have not been performed due to the need for detailed description of the vacancy formation process. Therefore, it is of interest to elucidate, which of the two scenarios of the vacancy formation is favorable.

Within the Schottky scenario, an atom is extracted from the surface of a perfect sphere, and in the final state the vacancy is in the center of the sphere. In this case, we have

$$\varepsilon_{N,v}^{\text{vac,Sh}} = [E_{N-1,v} + E_{\text{at}}] - E_N = N\varepsilon_N^{\text{coh}} - (N-1)\varepsilon_{N-1,v}^{\text{coh}}, \quad (63)$$

where $E_{N-1,v}$ is the total energy of sphere with vacancy (the spherical layer between $r = r_0$ and $r = R_{N-1,v}$ contains $N-1$ atoms).

According to another scenario [51], the number of atoms does not change, but the ‘‘bubble’’ of radius r_0 is blown in the center of the system. In this case, we have

$$\varepsilon_{N,v}^{\text{vac,blow}} = E_{N,v} - E_N = N(\varepsilon_N^{\text{coh}} - \varepsilon_{N,v}^{\text{coh}}). \quad (64)$$

The comparison of Eqs. (63) and (64) demonstrates the advantage of the second mechanism by relation

$$\varepsilon_{N,v}^{\text{vac,Sh}} = \varepsilon_{N,v}^{\text{vac,blow}} + \varepsilon_{N,v}^{\text{dis}}. \quad (65)$$

We construct the asymptotics of the monovacancy-formation energy. Its size dependence is determined by the difference in the total energies of the spheres calculated by the formulas (63) and (64) in the limit $N \rightarrow \infty$, and reduces to the difference of total surface energies.

For the vacancy blowing mechanism, using (5), we obtain

$$\begin{aligned}\varepsilon_{N,v}^{\text{vac,blow}} &= 4\pi R_{N,v}^2 \sigma_0 \left(1 + \frac{\delta_1}{R_{N,v}} + \frac{\delta_2}{R_{N,v}^2}\right) \\ &+ \varepsilon^{\text{vac}}(r_0) - 4\pi R_N^2 \sigma_0 \left(1 + \frac{\delta_1}{R_N} + \frac{\delta_2}{R_N^2}\right) \\ &= \varepsilon^{\text{vac}}(r_0) \left(1 + \frac{2}{3N^{1/3}(1 - \tilde{\delta}_1 + \tilde{\delta}_2)}\right).\end{aligned}\quad (66)$$

or the Schottky mechanism, in accordance with (65) and $R_{N-1,v} = R_N$, the asymptotics are determined by the sum of the expressions (66) and (59). Asymptotic dependence $\varepsilon_{N,v}^{\text{vac,Sh}}$ weakly depends on N , and the dependence (66) demonstrates a decrease in vacancy formation energy with an increase of N , which agrees with the conclusions of the paper [67, 68], but it contradicts the conclusions of Refs. [9–11].

The asymptotic size behavior of the vacancy formation energy (66) can be qualitatively compared with the results of [67] in which the energies of the cluster with or without vacancy have been calculated on the basis of the tight-binding approximation. Representing the expression (66) in the form

$$\varepsilon_{N,v}^{\text{vac,blow}}/\varepsilon_\infty^{\text{vac}} = 1 + C/N^{1/3},$$

we obtained that the values $C = 1.21, 1.50$ and 1.03 for Na, Mg and Al, respectively, are qualitatively consistent to $C = 1.33$ and 1.46 for Cu and β -Ti from [67].

Fig. 9 shows the results of calculations of the monovacancy-formation energy by two mechanisms. These calculations confirm the formula (65), namely, the advantage of blowing a vacancy. All dependences experience strong fluctuations. For some N , especially for Al, the values $\varepsilon_{N,v}^{\text{vac,blow}}$ become negative in narrow ranges of N . Such areas are shown in Fig. 4 and above, the paper already contains comments on hierarchy of electronic states in such clusters.

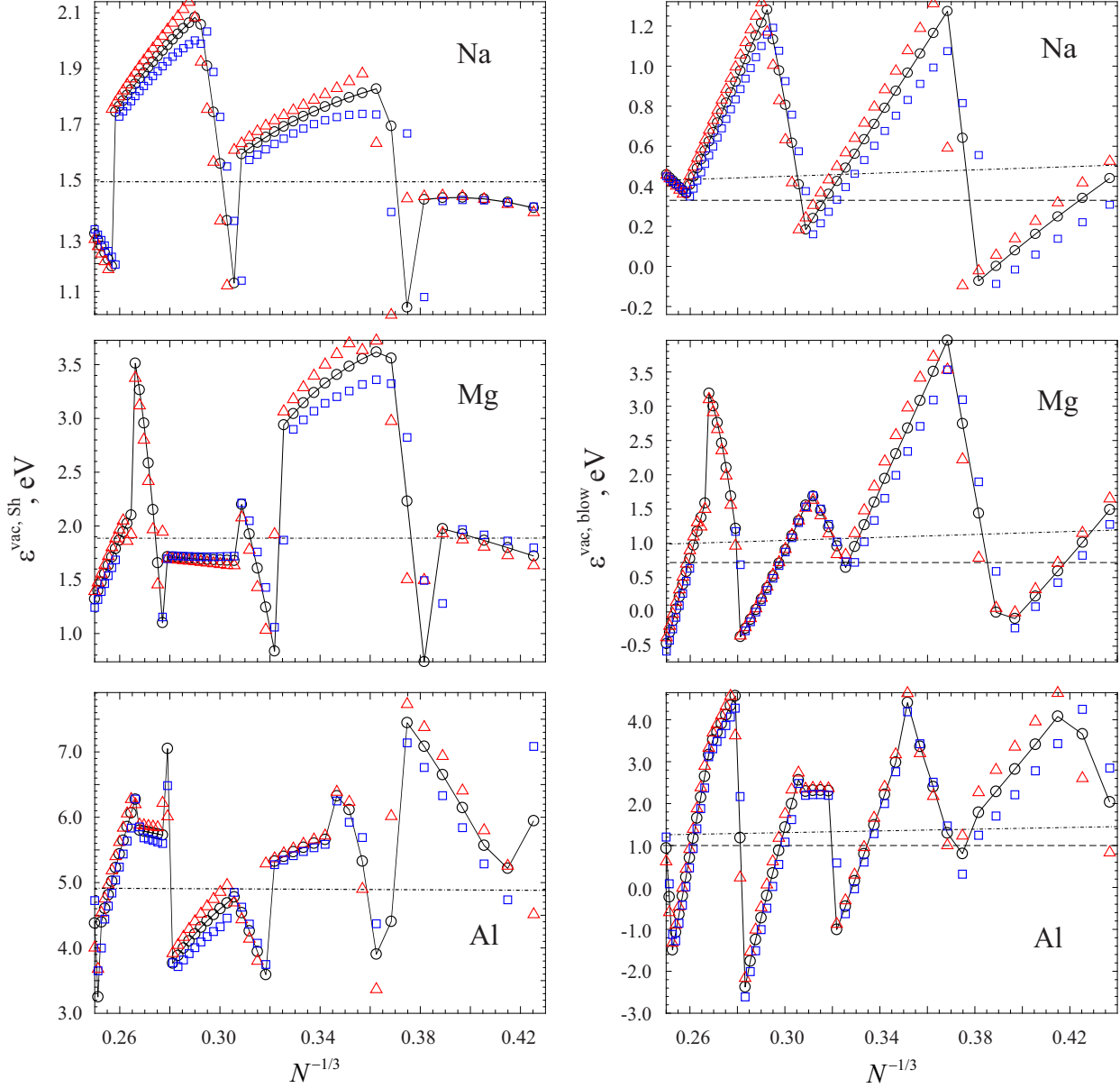


Figure 9: Computed quantities $\varepsilon_{N,v}^{\text{vac,Sh}}$ (63) and $\varepsilon_{N,v}^{\text{vac,blow}}$ (64) for clusters with a monovacancy (red triangles, black open circles, and blue open square correspond to positively charged, neutral, and negatively charged clusters, respectively); the black dash-dotted lines are asymptotics (65) and (66); horizontal black dashed lines (r. h. s.) correspond to $\varepsilon_{\infty}^{\text{vac}}$.

Table V. Monovacancy-formation energies (in eV) for neutral Na_N .

N	$\varepsilon_{N,v}^{\text{vac,Sh}}$		$\varepsilon_{N,v}^{\text{vac,blow}}$	
	This work	[32]	This work	[32]
55	1.80	1.35	0.49	0.49
147	1.58	1.18	0.66	0.43/0.63

The paper [32] reports on the results of ab initio calcu-

lations on $\text{Na}_{N=55,147,309}$ clusters that show icosahedral growth. The monovacancy-formation energy in cluster depends on the site at which the vacancy is created. A vacancy at the center or the first atom shell is found to cost much higher energy compared to other sites in the clusters.

In Table V, we compared the vacancy formation energy according to the Shottky mechanism (the atom is removed from the cluster center to outside) and according to the blowing bubble mechanism (the removed atom

is placed at the flat icosahedra surface [32]). On one hand, the comparison of $\varepsilon_{N,v}^{\text{vac,Sh}}$ (is denoted by E_r in Ref. [32]) reveals a difference of about 0.4 – 0.5 eV, but, on the other hand, it shows a similar size dependence. Values of $\varepsilon_{N,v}^{\text{vac,blow}}$ (is denoted by E_v in Ref. [32]) agree much better. In Table 5, in order to demonstrate the dependence of $\varepsilon_{N,v}^{\text{vac,blow}}$ on the location of vacancy formation, two values are presented, which are separated by the slash. They correspond to the atom displacement from the cluster center and from the first icosahedral atomic shell to the surface. The major aim of our simple treatment is not on the absolute values of clusters characteristics, but on their change upon vacancy formation.

The difference between the energies of formation of vacancies in a charged and neutral cluster in accordance with two scenarios ($E_N^\pm \rightarrow E_{N-1,v}^\pm + E_{\text{at}}$ and $E_N^\pm \rightarrow E_{N,v}^\pm$) by analogy with (61) can be represented in the form of relations

$$\begin{aligned}\Delta\varepsilon_{N,v}^{\text{vac,Sh,+}} &= \text{IP}_{N-1,v} - \text{IP}_N, \\ \Delta\varepsilon_{N,v}^{\text{vac,Sh,-}} &= \text{EA}_N - \text{EA}_{N-1,v}, \\ \Delta\varepsilon_{N,v}^{\text{vac,blow,+}} &= \text{IP}_{N,v} - \text{IP}_N, \\ \Delta\varepsilon_{N,v}^{\text{vac,blow,-}} &= \text{EA}_N - \text{EA}_{N,v}.\end{aligned}\quad (67)$$

The character of the size dependence $\varepsilon_{N,v}^{\text{vac,\pm}}$ (67) is fully supported by direct calculations and is determined by the behavior of IP and EA in Fig. 4.

The above calculations in LDA correspond to zero temperature. Perhaps, for a density of atoms corresponding to finite temperature, reduced symmetry of clusters, as well as the use of LSDA for exchange-correlation energy, strong oscillatory behavior of the energy characteristics will be suppressed. Anyway, the size behavior of the results of direct calculations agrees with its asymptotics.

In quasi-thermodynamics, the probability of the appearance of vacancies in a cluster at finite temperature T , can be estimated from the condition of free energy variation $\Delta F_{N,v}^{\text{vac,blow}}$,

$$\Delta F_{N,v}^{\text{vac,blow}} = \varepsilon_{N,v}^{\text{vac,blow}} - T\Delta S_{N,v}^{\text{vac,blow}} \leq 0. \quad (68)$$

As a result of the fact that when the vacancy is blown, the number of ions in the cluster does not change, the entropy contribution is provided only by the degenerate electron gas [69]. The corresponding expression is

$$\begin{aligned}T\Delta S_{N,v}^{\text{vac,blow}} &= \frac{2\pi^{5/3}}{3^{2/3}} \left(\frac{k_B T}{e^2} \right)^2 \\ &\times \int_0^\infty dr r^2 \left[n_{N,v}^{1/3}(r) - n_N^{1/3}(r) \right].\end{aligned}\quad (69)$$

For calculations in (69), equilibrium profiles of electron distributions in the stabilized jellium will be needed for given N and T . At zero temperature and $N = 12$ these profiles are presented on Fig. 3.

V. SUMMARY

In this paper, we propose a consistent formal procedure for finding ionization potential of a large metal cluster containing the vacancies that is based on a previously solved problem on the scattering of electrons by a monovacancy in bulk metal by the Kohn-Sham method in the stabilized jellium. Self-consistent profiles are used to determine the vacancy energy shift of the ground state in a metal cluster sphere as a series of size corrections. Spherical periodicity in the arrangement vacancies was assumed. The limits of applicability of this expansion to powers of the inverse radius are $R > 4.5$ nm and $R > 6$ nm for Na and Al, respectively.

In our work, the effect of bulk vacancies on the properties of a cluster is estimated. Only by introducing periodic arrangement of internal vacancies it is possible to consider the defected sample as a cellular media and to estimate the shift of its ionization potential. The presented approach seems to be promising for experimental estimation of the concentrations of bulk point defects or impurities in metal clusters. To this end, it is first needed to calculate the scattering length of electrons on the corresponding defect in 3D metal. The obtained analytical expressions are convenient for analysis of the results of photoionization experiments. In particular, the concentration of internal vacancies in a cluster formally can be estimated near the melting point using these expressions. The jellium and *ab initio* calculations [25, 27, 28, 32] reveal a rather subtle interplay between geometric and electronic shell effects, and evidences that the quantum mechanical description of the metallic bonding is crucial for understanding quantitatively the variation in melting temperatures observed experimentally for free clusters.

There is no doubt that the site of vacancies in the bulk, near or on the surface [32] will affect the characteristics of the cluster differently. And without a doubt it is difficult to determine their contribution separately. However, due to the fact that the concentration of equilibrium internal vacancies in 3D metals exponentially depends on the inverse temperature, the surface energy and work function will contain, in addition to the linear temperature dependences associated with thermal expansion, also the exponential dependence which is easier to observe near the melting of 3D metals. Due to the fact that the energy of the vacancy formation depends on its site in the cluster (on the surface it is approximately half the bulk), perhaps we should expect the weak exponential temperature dependences of their concentrations and, correspondingly, exponential temperature-dependent contribution to both IP and EA. The ability to distinguish and separate these dependences for large clusters or island films depends of course on the accuracy of the experiment.

The Fowler-Nordheim theory is applicable for planar field electron emission. As a modification, we can propose the use of the temperature and vacancy dependence of the electron work function. For special electrode ge-

ometry, adaptation of the theory is also possible in an analytical form (see, for example, [70]).

The self-consistent calculations of the electronic profiles for perfect clusters and clusters with a vacancy allowed us to determine the total energy of the neutral and charged defective cluster and then calculate the dissociation, cohesion, vacancy-formation energies, the ionization potential, and electron affinity as well as the electrical capacitance.

The results of calculations for Na and Al are compared with the asymptotics and results for defect-free clusters. The ionization potential for the smallest cluster with a vacancy is greater than for a perfect cluster (approximately 0.1 eV for Na and 0.5 eV for Al). A maximum difference is observed at the transition from a completely filled shell to the empty one. As N increases, this difference disappears.

Magic numbers of atoms for perfect clusters and clusters with monovacancy are different, especially for Al. Normalized electrical capacities of clusters always exceed unity and contain quantum size fluctuations. In this case, for defective clusters with partially filled electronic shells capacities are significantly larger than for perfect clusters.

The size dependence of the cohesion energy contains local maxima. Clusters corresponding to them are more stable, that is, have large-scale binding, dissociation, and vacancy-formation energies than their neighbors. For small clusters, such maxima appear at the complete filling of the next electron shell. The positions of the maxima for defect and defect-free clusters are different, which is due not only to the difference in their sizes, but also due to the character of the behavior of the electron wave functions.

The energy of cohesion of charged cluster anions and cations is different from the cohesive energy of neutral clusters. Excessive positive charge leads to a decrease in energy through increased forces of electrostatic repulsion, and excess negative charge leads to the opposite effect.

The quantum-size dependences of the vacancy-formation energies in the Schottky and the ‘‘bubble blowing’’ scenarios, and their asymptotic tendencies were determined. Strong size fluctuations in the entire cluster size range were found. Size asymptotics for these two mechanisms are different from each other and are weakly dependent on the number of atoms in the cluster. The nature of the size dependence of vacancy-formation energies from excess charge in a cluster is determined by the behavior of the ionization potential of the cluster and the electron affinity.

With the increase in N the dissociation energy is either increases, or has a local minimum (in the areas between the maxima), while the vacancy-formation energies decrease monotonically.

Figs. 7 – 9 indicate that all characteristics of charged and neutral clusters differ from each other. It is reasonable to assume that charging might control the melting temperature of the clusters (see experimental size depen-

dent melting temperature of anions and cations Al_{35–70} at Fig. 4 in [63]).

In this model, the relaxation of the cluster volume was not taken into account. In the limit of large clusters, the effect of self-compression on the ionization potential is analytically described in [42, 44], and for small clusters is numerically investigated in a spherically averaged pseudopotential model [26]. Relaxation of ionic distribution in the cluster will lead to a decrease in the total energy. More coherent, but also more labor-intensive, are *ab initio* methods with the selection of the coordinates of ions under the minimum condition of the total energy of the cluster. Such a procedure is implemented in [63] only for Al_{30–70} clusters, i.e., clusters with a small atoms number.

Acknowledgments

We are grateful to Walter V. Pogosov for reading the manuscript.

Appendix A: Vacancy quantum correction

The straightforward estimation for $\langle \delta V \rangle_{R_{N,v}}$ in (44) gives the surprising result:

$$\langle \delta V \rangle_{R_{N,v}} \approx \left\langle \left(R_v \frac{\nabla u_{WS}}{u_{WS}} \right) (R_{N,v} \psi \nabla \psi) \right\rangle \approx \frac{\hbar^2}{m R_v^2} \frac{R_v}{R_{N,v}}, \quad (\text{A1})$$

where $\langle \dots \rangle$ denotes the integration over the cluster volume. It seems as if $\langle \delta V \rangle_{R_{N,v}}$ is proportional to $(R_v R_{N,v})^{-1}$. In this case the hierarchy of terms in our expansion (42) would be broken, because the previous term is proportional to $R_{N,v}^{-2}$. However, below we shall demonstrate the emergence of an extra factor to $\langle \delta V \rangle_{R_{N,v}}$ which is proportional to $\xi (R_v/R_{N,v})$,

$$\xi = \frac{L_v}{R_v} \equiv \frac{L_v}{r_0} c_v^{1/3} \ll 1. \quad (\text{A2})$$

It is a result of the integration in Eq. (44) over angles [53].

Due to the fact that the perturbation $\delta V(r)$ occurs on a scale of supercell, in (44), it will be reasonable to proceed to integration over supercell and use the Green formula:

$$\begin{aligned} \langle \delta V \rangle_{R_{N,v}} &= -\frac{\hbar^2}{2m} \sum_{i=1}^{N_v} \int_{\Omega_i} d\mathbf{r} \nabla \left\{ \ln [u_{WS}(\varrho)] \right\} \nabla \psi^2(r) \\ &= -\frac{\hbar^2}{2m} \sum_{i=1}^{N_v} \left[\ln u_{WS} \Big|_{\varrho=R_v} \oint_{S_i} d\mathbf{S} \nabla \psi^2 \right. \\ &\quad \left. - \int_{\Omega_i} d\mathbf{r} \ln u_{WS} \nabla^2 \psi^2 \right], \quad (\text{A3}) \end{aligned}$$

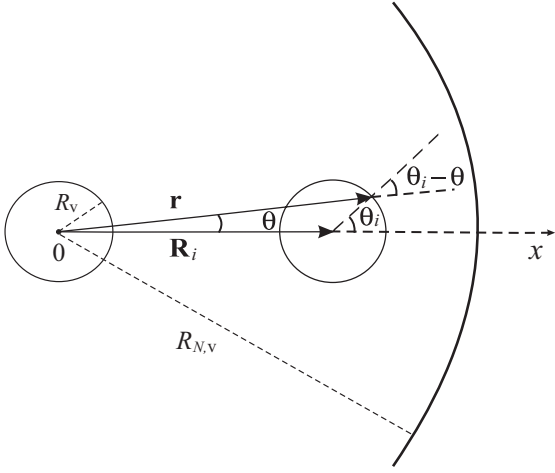


Figure 10: The scheme for calculation of the integral over surface of i th cell.

where Ω_i is a volume of space under condition $L_v < \varrho < R_v$.

Let us introduce the gradient expansion of the squared wave function $\psi^2(r)$ near the point \mathbf{R}_i ,

$$\begin{aligned} \psi^2(r) &= \psi^2(r) \Big|_{r=R_i} + \nabla \psi^2(r) \Big|_{r=R_i} (\mathbf{r} - \mathbf{R}_i) \\ &+ \frac{1}{2} \nabla^2 \psi^2(r) \Big|_{r=R_i} (r^2 - 2\mathbf{r}\mathbf{R}_i + R_i^2) + \dots \end{aligned} \quad (\text{A4})$$

Using expansions of derivatives over the small parameter $\varrho/R_i \equiv R_v/R_i$ we can take the derivatives over \mathbf{r} at the centers of cells \mathbf{R}_i ,

$$\begin{aligned} \nabla \psi^2(r) \Big|_{R_i \gg R_v} &= \left[\frac{d\psi^2(R_i)}{dR_i} + \frac{d^2\psi^2(R_i)}{dR_i^2} \frac{R_v}{R_i} \right] \frac{\mathbf{r}}{r} \\ &= \frac{d\psi^2(R_i)}{dR_i} \left[1 + O\left(\frac{R_v^2}{R_i^2}\right) \right] \frac{\mathbf{r}}{r}, \end{aligned} \quad (\text{A5})$$

and

$$\nabla^2 \psi^2(r) \Big|_{R_i \gg R_v} = \nabla^2 \psi^2(r) \Big|_{r=R_i} + O\left(\frac{R_v^3}{R_i^3}\right). \quad (\text{A6})$$

Then

$$\begin{aligned} \langle \delta V \rangle_{R_{N,v}} &= -\frac{\hbar^2}{2m} \sum_{i=1}^{N_v} \left[\frac{d\psi^2(R_i)}{dR_i} (\ln u_{\text{WS}}) \Big|_{r=R_v} \oint_{S_i} d\mathbf{S} \frac{\mathbf{r}}{r} \right. \\ &\quad \left. - \nabla^2 \psi^2(r) \Big|_{r=R_i} \int_{\Omega_i} d\mathbf{r} \ln u_{\text{WS}} \right]. \end{aligned} \quad (\text{A7})$$

Using expression (16), we obtain

$$(\ln u_{\text{WS}}) \Big|_{r=R_v} = -\frac{3}{2}(\xi - \xi^2) + O(\xi^3). \quad (\text{A8})$$

The terms under the sum in Eq. (A7) have the opposite signs.

The integral over the surface of i th cell is evaluated exactly (see Fig. 10),

$$\begin{aligned} \oint_{S_i} d\mathbf{S} \frac{\mathbf{r}}{r} &= 2\pi R_v^2 \int_0^\pi d\theta \cos(\theta_i - \theta) \sin \theta_i \\ &= 2\pi R_v^2 \begin{cases} 1 - \frac{1}{3} \frac{R_i}{R_v}, & R_i < R_v, \\ \frac{2}{3} \frac{R_v}{R_i}, & R_i > R_v. \end{cases} \end{aligned} \quad (\text{A9})$$

Hence, the integration over angles at $R_i \gg R_v$ gives the additional power of R_v/R_i . Now, taking account for the factor R_v/R_i from Eq. (A9), we replace in Eq. (A7) summation by integration and obtain

$$\sum_{i=1}^N \frac{d\psi^2}{dR_i} \frac{1}{R_i} = \frac{3}{R_v^3} \int_0^{R_N} dr r \frac{d\psi^2(r)}{dr} = -\frac{3D_0}{2R_v^3 R_{N,v}^2}, \quad (\text{A10})$$

$$D_0 = -\int_0^\pi d\varphi \left(\frac{\sin 2\varphi}{2\varphi} - \frac{\sin^2 \varphi}{\varphi^2} \right) \approx 0.71.$$

Next, after the change of the summation over cell numbers to the integration over the cluster volume it is possible to reduce the second term in (A7) to a surface integral. The integral vanishes due to the boundary condition (41). Finally, using Eqs. (A9) and (A10), we have first nonzero term

$$\langle \delta V \rangle_{R_{N,v}} = -\frac{\hbar^2 \pi^2}{2m R_{N,v}^2} D_1 \xi + O\left(\frac{\xi^2}{R_{N,v}^2}, \frac{R_v^3}{R_{N,v}^3}\right), \quad (\text{A11})$$

where $D_1 = 12D_0/\pi$. It is worth noting that the excluded volumes inside the supercells contribute to neglected terms $\sim \xi^3$.

-
- [1] Y. I. Frenkel, *Kinetic Theory of Liquids* (Clarendon Press, Oxford, 1946).
- [2] A. R. Ubbelohde, *The Molten State of Matter* (Wiley, Chichester, 1978).
- [3] R. S. Berry and B. M. Smirnov, *Phys. Rep.* **527**, 205 (2013).
- [4] A. V. Babich, V. V. Pogosov, and V. I. Reva, *Phys. Solid State* **57**, 2135 (2015).
- [5] V. Z. Kresin and Y. Ovchinnikov, *Phys. Rev. B* **74**, 024514 (2006).
- [6] A. Halder and V. V. Kresin, *Phys. Rev. B* **92**, 214506 (2015).
- [7] J. R. Sambles, L. M. Skinner, and N. D. Lisgarten, *Proc. R. Soc. Lond. A* **318**, 507 (1970); J. R. Sambles, *Proc. R. Soc. Lond. A* **324**, 339 (1971).
- [8] Ph. Buffat and J.-P. Borel, *Phys. Rev. A* **13**, 2287 (1976).
- [9] C. C. Yang and S. Li, *Phys. Rev. B* **75**, 165413 (2007).
- [10] S. C. Hendy, *Nanotechnology* **18**, 175703 (2007).
- [11] G. Guisbiers, *Nanoscale Res. Lett.* **5**, 1132 (2010).
- [12] A. Safaei, *Phil. Mag.* **91**, 1509 (2011).
- [13] W. Luo, K. Su, K. Li, G. Liao, N. Hu, and M. Jia, *J. Chem. Phys.* **136**, 234704 (2012).
- [14] J. Chandra and K. Kholiya, *Mod. Phys. Lett. B* **29**, 1550025 (2015).
- [15] W. Qi, *Acc. Chem. Res.* **49**, 1587 (2016).
- [16] G. A. Breaux, C. M. Neal, B. Cao, and M. F. Jarrold, *Phys. Rev. Lett.* **94**, 173401 (2005).
- [17] C. Hock, C. Bartels, S. Straßburg, M. Schmidt, H. Haberland, B. von Issendorff, and A. Aguado, *Phys. Rev. Lett.* **102**, 043401 (2009).
- [18] A. K. Starace, B. Cao, O. H. Judd, I. Bhattacharyya, and M. F. Jarrold, *J. Chem. Phys.* **132**, 034302 (2010).
- [19] S. Zamith, P. Labastie, F. Chiro, and J.-M. L'Hermite, *J. Chem. Phys.* **133**, 154501 (2010).
- [20] C. Bréchnac, Ph. Cahuzac, J. Leygnier, and J. Weiner, *J. Chem. Phys.* **90**, 1492 (1989).
- [21] U. Ray, M. F. Jarrold, J. E. Bower, and J. S. Kraus, *J. Chem. Phys.* **91**, 2912 (1989).
- [22] A. Halder and V. V. Kresin, *J. Chem. Phys.* **143**, 164313 (2015).
- [23] W. A. de Heer, *Rev. Mod. Phys.* **65**, 611 (1993).
- [24] M. Brack, *Rev. Mod. Phys.* **65**, 677 (1993).
- [25] C. Yannouleas and U. Landman, *Phys. Rev. B* **51**, 1902 (1995).
- [26] A. Vieira, M. B. Torres, C. Fiolhais, and L. C. Balbás, *J. Phys. B* **30**, 3583 (1997).
- [27] J. Akola, M. Manninen, H. Häkkinen, U. Landman, X. Li, and L.-S. Wang, *Phys. Rev. B* **62**, 13216 (2000).
- [28] S. Chacko, D. G. Kanhere, and S. A. Blundell, *Phys. Rev. B* **71**, 155407 (2005).
- [29] A. Aguado and J. M. López, *J. Chem. Phys.* **130**, 064704 (2009).
- [30] J. P. Perdew, H. Q. Tran, and E. D. Smith, *Phys. Rev. B* **42**, 11627 (1990).
- [31] C. Baladrón, J. A. Alonso, and M. P. Iñiguez, *Phys. Rev. B* **37**, 8436 (1988).
- [32] M. Itoh, V. Kumar, and Y. Kawazoe, *Phys. Rev. B* **73**, 035425 (2006).
- [33] P. Ziesche, J. P. Perdew, and C. Fiolhais, *Phys. Rev. B* **49**, 7919 (1994).
- [34] M. Seidl and M. Brack, *Ann. Phys.* **245**, 275 (1996).
- [35] M. Seidl, J. P. Perdew, M. Brajczewska, and C. Fiolhais, *J. Chem. Phys.* **108**, 8182 (1998).
- [36] A. V. Babich, P. V. Vakula, and V. V. Pogosov, *Phys. Solid State* **56**, 873 (2014).
- [37] A. V. Babich, P. V. Vakula, and V. V. Pogosov, *Phys. Solid State* **56**, 1726 (2014).
- [38] S. Amelinckx and D. Van Dyck, in *Encyclopedia of Materials Science and Engineering*, edited by R. W. Cahn (Pergamon, New York, 1988), Vol. 1, p. 77.
- [39] I. T. Iakubov, A. G. Khrapak, L. I. Podlubny, and V. V. Pogosov, *Sol. St. Commun.* **53** 427 (1985).
- [40] V. V. Pogosov, *Sol. St. Commun.* **75**, 469 (1990).
- [41] V. V. Pogosov, *Phys. Solid State* **35**, 518 (1993).
- [42] I. T. Iakubov and V. V. Pogosov, *Physica A* **214**, 287 (1995).
- [43] V. V. Pogosov, *Phys. Solid State* **37**, 1547 (1995).
- [44] A. Kiejna and V. V. Pogosov, *J. Phys.: Cond. Matter.* **8**, 4245 (1996).
- [45] T. P. Martin, *Phys. Rep.* **273**, 199 (1996).
- [46] A. V. Babich, unpublished.
- [47] B. E. Springett, M. H. Cohen, and J. Jortner, *Phys. Rev.* **159**, 183 (1967).
- [48] J. Bardeen, *J. Chem. Phys.* **6**, 367 (1938).
- [49] M. H. Cohen and F. S. Ham, *J. Phys. Chem. Sol.* **16**, 177 (1960).
- [50] M. J. Stott and P. Kubica, *Phys. Rev. B* **11**, 1 (1975).
- [51] V. V. Pogosov, *Sol. St. Commun.* **89**, 1017 (1994).
- [52] E. M. Gullikson and A. P. Mills, Jr, *Phys. Rev. B* **35**, 8759 (1987).
- [53] V. V. Pogosov and V. I. Reva, *Phys. Solid State* **59**, 1063 (2017).
- [54] A. Kawabata and R. Kubo, *J. Phys. Soc. Jpn.* **21**, 17 (1966).
- [55] V. Pogosov, V. P. Kurbatsky, and E. V. Vasyutin, *Phys. Rev. B* **71**, 195410 (2005).
- [56] M. A. Hoffmann, G. Wrigge, and B. von Issendorff, *Phys. Rev. B* **66**, 014404 (2002).
- [57] J. A. Alonso and N. M. March, *Surf. Sci.* **160**, 509 (1985).
- [58] O. Kostko, Ph.D. dissertation (University of Freiburg, 2007).
- [59] W. Ekardt, *Phys. Rev. B* **29**, 1558 (1984).
- [60] J. P. Perdew, in *Condensed Matter Theories, Vol. 4*, edited by J. Keller (Plenum, New York, 1989).
- [61] J. R. Sabin, S. B. Trickey, S. P. Apell, and J. Oddershede, *Int. J. Quant. Chem.* **77**, 358 (2000).
- [62] V. V. Pogosov, *Phys. Solid State* **36**, 1371 (1994).
- [63] A. K. Starace, C. M. Neal, B. Cao, M. F. Jarrold, A. Aguado, and J. M. López, *J. Chem. Phys.* **131**, 044307 (2009).
- [64] M. E. Garcia, D. Reichardt, and K. H. Bennemann, *J. Chem. Phys.* **109**, 1101 (1998).
- [65] C. Freysoldt, B. Grabowski, T. Hickel, J. Neugebauer, G. Kresse, A. Janotti, and C. G. Van de Walle, *Rev. Mod. Phys.* **86**, 253 (2014).
- [66] Y. Kraftmakher, *Phys. Rep.* **299**, 79 (1998).
- [67] M. Sinder, D. Fuks, and J. Pelleg, *Phys. Rev. B* **50** 2775 (1994).
- [68] H. Delavari, H. R. Madaah Hosseini, and A. Simchi, *Physica B* **406**, 3777 (2011).
- [69] N. W. Ashcroft and D. Stroud, *Solid State Phys. (Acad. Press, N.Y.)* **33**, 1 (1978).

- [70] K. Yuasa, A. Shimoi, I. Ohba, C. Oshima, *Surf. Sci.* **520**, 18 (2002).